Elsevier Editorial System(tm) for Geochimica et Cosmochimica Acta
Manuscript Draft

Manuscript Number: W7857R2

Title: (W7857)Complex magmatic and impact history prior to 4.1 Ga recorded in zircon from Apollo 17 South Massif aphanitic breccia 73235.

Article Type: Article

Corresponding Author: Dr Marion Grange,

Corresponding Author's Institution: Curtin University of Technology

First Author: Marion Grange

Order of Authors: Marion Grange; A A Nemchin; N Timms; R T Pidgeon; C Meyer

Abstract: Sample 73235 is one of several aphanitic impact melt breccias collected by the Apollo 17 mission at stations 2 and 3 on the slopes of the South Massif. This study presents a detailed investigation of internal structures and U-Pb ages of large zircon grains from this breccia sample. New data combined with the results of previous studies of zircon grains from the same location indicate that most zircon clasts in breccias from stations 2 and 3 formed during multiple magmatic events between 4.37 and 4.31 Ga, although the oldest zircon crystallized at about 4.42 Ga and the youngest at 4.21 Ga. In addition, zircons from the aphanitic breccias record several impact events prior to the ~3.9 Ga Late Heavy Bombardment. The results indicate that the zircons probably crystallized at different locations within the Procellarum KREEEP Terrane and were later excavated and modified by several impacts and delivered to the same locality within separate ejecta blankets. This locality became a source of material that formed the aphanitic impact melt breccias of the South Massif during a ~3.9 Ga impact. However, the zircons, showing old impact features, are not modified by this ~3.9 Ga impact event suggesting that (i) this common source area was located at the periphery of excavation cavity, and (ii) the > 3.9 Ga ages recorded by the zircon grains could date large (basin-forming) events as significant as major later (~3.9 Ga) collisions such as Imbrium and Serenitatis.

Complex magmatic and impact history prior to 4.1 Ga recorded in zircon from Apollo 17 South Massif aphanitic breccia 73235.

M.L. Grange[1 *], A.A. Nemchin[1,2], N. Timms[1], R.T. Pidgeon[1], C. Meyer[3]

[1]Department of Applied Geology, Western Australian School of Mines, Curtin University, GPO Box U1987, Western Australia, 6845, Australia

[2] Institute für Mineralogie, Münster University, Correnstrasse 24, D-48149, Münster, Germany

[3] NASA Johnson Space Center, Houston, TX 77058, USA

** corresponding author:|e-mail| m.grange@curtin.edu.au; |tel| +61 8 9266 7969*

ABSTRACT

Sample 73235 is one of several aphanitic impact melt breccias collected by the Apollo 17 mission at stations 2 and 3 on the slopes of the South Massif. This study presents a detailed investigation of internal structures and U-Pb ages of large zircon grains from this breccia sample. New data combined with the results of previous studies of zircon grains from the same location indicate that most zircon clasts in breccias from stations 2 and 3 formed during multiple magmatic events between 4.37 and 4.31 Ga, although the oldest zircon crystallized at about 4.42 Ga and the youngest at 4.21 Ga. In addition, zircons from the aphanitic breccias record several impact events prior to the ~3.9 Ga Late Heavy Bombardment. The results indicate that the zircons probably crystallized at different locations within the Procellarum KREEEP Terrane and were later excavated and modified by several impacts and delivered to the same locality within separate ejecta blankets. This locality became a source of material that formed the aphanitic impact melt breccias of the South Massif during a ~3.9 Ga impact. However, the zircons, showing old impact features, are not modified by this ~3.9 Ga impact event suggesting that (i) this common source area was located at the periphery of excavation cavity, and (ii) the > 3.9 Ga ages recorded by the zircon grains could date large (basin-forming) events as significant as major later (~3.9 Ga) collisions such as Imbrium and Serenitatis.

Key words: Lunar zircon; impact and igneous events; U-Pb dating; zircon internal texture; zircon deformation; EBSD.

1. INTRODUCTION

The Taurus-Littrow Valley, located between two highland massifs called the South and North massifs (Wolfe et al., 1981) was selected as the Apollo 17 landing site because it lies just outside the transient cavity of the Serenitatis impact basin (Head, 1979; Ryder et al., 1997) and is interpreted to overlie the upper part of thick ejecta from this impact (e.g., Wolfe et al., 1981). This is consistent with the composition of boulders at the base of the South Massif which consist of texturally heterogeneous breccias (Simonds, 1975). These breccias are interpreted to be impact melt breccias based on the texture and composition of their matrices which correspond to crystallized impact melt. They are subdivided into two different groups: (1) more abundant poikilitic matrix breccias, which are ubiquitous throughout the landing site and (2) aphanitic matrix breccias, which are found mostly at the South Massif and mainly represented by Boulder 1 from Station 2 (e.g., Spudis and Ryder, 1981; Ryder, 1993), although, Jolliff et al. (1996) reported small lithic fragments belonging to the aphanitic group at Station 6 (North Massif). Differences between two breccias groups are highlighted by:

(i) The grain size of their matrices;

(ii) The abundance of clasts and clast populations: poikilitic breccias contain a relatively small proportion of clasts derived mostly from relatively deep-seated Mg-suite rocks (Ryder et al., 1975; Spudis and Ryder, 1981; Wolfe et al., 1981; Ryder, 1993), while aphanitic samples show a larger proportion and diversity of clasts, including some higher level rocks such as granulite and felsic clasts (e.g., Simonds, 1975; Spudis and Ryder, 1981; Jolliff et al., 1996);

(iii) Major and trace element concentrations of the matrices: aphanitic breccias show a larger range of chemical variations and are especially distinguished from the poikilitic melts by their lower Ti and higher Al content (Spudis and Ryder, 1981), as well as lower Na_2O, Sr and Eu concentrations (Jolliff et al., 1996). Jolliff et al. (1996), who investigated small (few mm) lithic fragments preserved in the Apollo 17 soil samples, also identified impact melts compositionally different from those preserved in both aphanitic and poikilitic breccias. Compared to the two main groups, these impact melts are glassy to cryptocrystalline, enriched in incompatible elements and show lower Mg' and Cr/Sc, and high Sm/Eu (Jolliff et al., 1996). These melts,

however, are restricted to the small particles extracted from the soil samples and, to date, have not been identified in the breccia samples.

It has been suggested that in addition to textural and chemical differences, the poikilitic and aphanitic impact melt breccias also have different ages (see summary in Stöffler et al., 2006). Dalrymple and Ryder (1996) concluded that the poikilitic impact melt breccias represent the Serenitatis event and their best estimated ^{40}Ar-^{39}Ar age of 3893 ± 9 Ma (1σ) for the breccias is widely accepted as the age of the Serenitatis basin. Aphanitic impact melts proved to be more difficult to date. The first attempts to determine their age (e.g., Leich et al., 1975; Schaeffer et al., 1982) were very imprecise. The best currently available ages of aphanitic impact melt fractions, also obtained by Dalrymple and Ryder (1996), range between 3869 ± 16 and 3951 ± 17 Ma (1σ). From these data, it is not possible to identify a clear age difference between poikilitic and aphanitic melt breccias.

Chemical and textural differences observed between the two types of Apollo 17 breccias led some authors to conclude that poikilitic and aphanitic melts represent different impacts (e.g., Ryder et al., 1975; Spudis and Ryder, 1981; Dalrymple and Ryder; 1996; see summary in Rockow and Haskin, 1996). A common interpretation is that the poikilitic impact melt breccias represent Serenitatis ejecta while the aphanitic breccias could be associated with the Imbrium event or a smaller unidentified impact. However, others highlighted similarities between the two breccias types (e.g., Wood, 1975; Winzer et al., 1977; James et al., 1978; Wolfe et al., 1981 and references therein), arguing that textural differences can be explained by the different cooling histories of the samples, while subtle chemical variations could be related to the heterogeneity of the target in a single impact. An extreme view, expressed by Haskin et al. (1998), is that the overall variation of chemical compositions of breccia samples in the Apollo collection is relatively small and all Apollo landing sites are heavily dominated by Imbrium ejecta. A region on the near side of the Moon with a significant Th concentration, termed Procellarum KREEP Terrane (PKT) by Jolliff et al. (2000), corresponds approximately to what is known as the Procellarum Ocean and is interpreted as representing a KREEP-rich zone (KREEP stands for enriched K, REE and P). Impact melt breccias showing high concentrations of incompatible elements most likely originated from within the PKT and may be related to the Imbrium basin located in the center of the terrane.

However, on present evidence, the provenances of Apollo breccia samples remains controversial and further work is needed to resolve the issue. Precise chronology is essential to date different types of impact melts, and to investigate the origin and history of clasts preserved in the samples. This will enable a comparison of source regions of different breccias types (poikilitic vs. aphanitic), leading to the characterization of target areas of impacts and therefore helping to determine which impacts produced specific types of breccias samples. The presence of zircon in a number of aphanitic breccias from the South Massif, both in the matrix and in lithic clasts, offers the possibility of constraining the timing of the magmatic and impact history of clast populations as well as the origin of the breccia samples. Where they are affected by a severe impact, zircons can record the age of impact. However, the zircon record provides an incomplete record of the history of a region, as it may not necessarily reflect every magmatic event in the source region and will only record impacts that are sufficiently large to severely affect the U-Pb stability of existing grains. Nevertheless, zircons have the potential to provide highly significant information on both crust formation and impact chronology of Apollo 17 melt breccias.

With that in mind, we have investigated the timing of magmatic and impact events recorded in zircon clasts from the aphanitic breccia sample 73235, from the Apollo 17 South Massif. We combine these results with U-Pb ion probe measurements of zircons from other breccias from the South Massif and construct the timing of igneous and impact events in this part of the lunar crust. Finally, this paper discusses the implications of our results for the conclusions about the nature and complexity of the lunar crust, as well as the provenance of Apollo 17 aphanitic breccia samples.

2. BRECCIA SAMPLES FROM THE SOUTH MASSIF

Apollo 17 Station 3 (Figure 1a-b) is located within the light mantle landslide material from the South Massif. Breccia samples, 73235 and 73217, were collected from the rim of a 10m crater. Breccia 73235 is classified as fine-grained clast-rich aphanitic impact melt breccias (Spudis and Ryder, 1981; Ryder, 1993). It is composed of a dense aphanitic melt groundmass with a seriate clast distribution (Ryder, 1993).

142 The groundmass consists of plagioclase, pyroxene, opaque minerals and rare spinel.
143 The lithic clasts are dominated by highland rock types (shocked Mg-suite anorthosites
144 and cataclasized troctolites and norites) strung out as schlieren within the dense
145 matrix (Ryder, 1993), with no mare basalt clasts (e.g., Dence et al., 1976; Warren and
146 Wasson, 1979). Sample 73235 is very similar to 73215 (Ryder, 1993), which has been
147 extensively studied by a consortium led by O. James (e.g., James et al., 1975; James
148 and Blanchard, 1976). The chemistry of the aphanitic matrix is consistent with an
149 aluminous, low K-Fra Mauro (LKFM; for definition and details see Korotev, 1994)
150 basalt composition.
151 The other sample from Apollo 17 Station 3 investigated in this study is breccia
152 73217, first described by Ishii et al. (1983) as a calcic-plagioclase-rich micro-breccia
153 containing abundant angular mineral clasts and rare lithic clasts in a fine-grained
154 matrix, partially made of glass. This sample also contains one of the rare ferroan
155 anorthosite clasts of the Apollo 17 sample collection (Warren et al., 1983). The
156 composition of the glass was found to be very felsic and K-rich (Huber and Warren,
157 2008), with no chemical equilibrium between the clasts and the melt, suggesting the
158 absence of a genetic link between them. Long blades of ilmenite, Ca-phosphate and
159 zircon appear to have crystallized from the felsic glass (Huber and Warren, 2008;
160 Grange et al., 2009). Grange et al. (2009) suggested that the glass represents a felsic
161 melt quenched by an impact and that the zircon grains crystallized from this melt
162 determine the age of the impact.
163 We have also included in this study three aphanitic impact melt breccia
164 samples from Station 2, 72215, 72255 and 72275, which were chipped from Boulder
165 1 interpreted to have slid down the slope of the South Massif (Figure 1c-d). This
166 boulder has been studied by the Consortium Indomitabile lead by Wood (e.g., Marvin,
167 1975; Wood, 1975; Ryder et al., 1975). It consists of two main parts (see summary in
168 Wolfe et al., 1981): a light-grey friable feldspar-rich matrix (e.g., sample 72275) and a
169 dark-grey competent microbreccia (72215 and 72275, and clast within 72275). The
170 dark grey part is interpreted as an older impact breccia incorporated into the light grey
171 matrix (Wolfe et al., 1981). The lithic clasts of the boulder are dominated by ANT
172 fragments and granulitic breccias (e.g., recrystallized older breccias), however sample
173 72275 also contains a KREEP basalt and a rare FAN fragment (Salpas et al., 1988).
174 The presence of substantial amount of zircon grains in these breccias as
175 compared to rare occurrence of zircon in poikilitic impact breccias can be taken as an

independent support of their different origin. However, it can also reflect the substantially larger overall concentration of clasts in aphanitic melt breccias, rather than difference in the target area for the poikilitic and aphanitic breccias. Regardless of the origin of aphanitic breccias, presence of zircon in these samples gives an opportunity to obtain additional information about variability of lunar crust prior to ~3.9 Ga bombardment.

3. ANALYTICAL TECHNIQUES

3.1. Scanning Electron Microscope (SEM) and Electron Backscatter Diffraction (EBSD) imaging

The zircon grains and their petrographic setting were characterized using backscattered electron (BSE), secondary electron (SE) and panchromatic cathodoluminescence (CL) imaging obtained with the scanning electron microscope (SEM) at the Microstructural Analysis Facility, Curtin University of Technology, Western Australia. Petrographic polished thin sections were given a final polish with 0.06 μm colloidal silica NaOH suspension (pH 9.8) for ~4 hours on a Buehler Vibromet II polisher. A thin (~1nm) carbon coat was applied before SEM analyses to reduce surface charging. BSE and CL images were collected using a W-source Philips XL30 SEM fitted with a CCD-Si collector. SE images were collected using a Zeiss NEON field emission SEM.

The internal microstructure of the zircon grains was quantified by electron backscatter diffraction (EBSD) analysis. EBSD mapping involves the collection of electron backscatter diffraction patterns (EBSPs) at points on a user defined grid from a highly polished surface that is free of mechanical damage. Analysis of fundamental properties of the EBSPs, such as the strength of the diffraction (Kikuchi) bands can provide valuable qualitative information on crystallographic damage (Cayzer et al., 2008; Lehockey et al., 2000; Tucker et al., 2000; Wilkinson, 2000; Timms et al., 2010). Diffraction bands in the patterns were automatically detected and used to fit a solution. Indexing of the patterns in this way quantifies the mineral phase and full crystallographic orientation at each point and permits the generation of maps and other plots of orientation data (Prior et al., 2009). EBSD data were collected using an

Oxford Instruments EBSD acquisition system fitted to a Zeiss Neon SEM at Curtin University. All EBSD data were processed using Oxford Instruments Channel 5 (SP9) software using procedures detailed elsewhere (Reddy et al., 2007). Indexing of empirical EBSPs utilized match unit optimization outlined by Reddy et al. (2008), yielding >90% indexing and mean angular deviation of each EBSP solution of 0.3-0.5°. Cumulative misorientation maps were generated to show orientation variations across zircon by coloring each pixel for misorientation from a user-defined reference orientation of the grain, and show absolute orientation variations within a grain (Reddy et al., 2007).

3.2. Sensitive High Resolution Ion Micro-Probe (SHRIMP)

Uranium-lead isotopic data were collected with the Sensitive High Resolution Ion Microprobe (SHRIMP II) located in the John de Laeter Centre of Mass Spectrometry (Perth, Western Australia). The SHRIMP methodology follows analytical procedures described elsewhere (Williams, 1998). The filtered O_2^- primary ion beam, with initial intensity between 2 and 3 nA, was reduced through Kohler aperture of 70 μm to obtain a focused spot on the surface of samples of about 10 μm. This reduction results in a decrease in intensity to ~1.5 nA. Secondary ions were passed to the mass spectrometer operating at a mass resolution (M/ΔM at 1%) of ~5000. Each analysis was preceded by a 2 minutes raster to remove the Au coating and surface contamination.

The peak-hopping U-Pb data collection routine consisted of seven scans through the mass stations, with signals measured by an ion counting electron multiplier. Pb/U were calibrated using an empirical correlation between Pb^+/U^+ and UO^+/U^+, normalised to the 564 Ma Sri-Lankan zircon CZ3 (Pidgeon et al., 1994). The 1.6% external 1-sigma error, obtained during SHRIMP session from the multiple analyses of Pb/U on the zircon standard was added in quadrature to the errors observed in the unknowns. The initial data reduction was done using the SQUID 2 add-in for Microsoft Excel and Isoplot was applied for further age calculations (Ludwig, 2003a; 2003b). All errors for the U-Pb data obtained on individual SHRIMP spots are shown as 1-sigma (unless specified), while errors of average, concordia and intercept ages are given at the 95% confidence level.

4. RESULTS

U-Pb data from zircon grains are reported in Table 1. The largest and more complex grains of this study have been assigned a reference nickname based on their physical appearance to facilitate discussion.

4.1. Zircon 73235,60#4 – 'the hexagon'

This zircon is an isolated mineral clast enclosed in the breccia matrix (composed mainly of plagioclase and pyroxene) and surrounded by small radiating cracks (Figure 2a), probably related to the volume expansion of zircon as it accumulated radiation damage. This is one of the least complex grains in the studied lunar samples: it is not zoned and has a smooth and homogenously polished surface (Figure 2b). The subhedral form of this zircon suggests it had little abrasion during transport and inclusion within the breccia matrix. However, a narrow zone along one edge of the grain has high relief in the SE image (i.e., is more resistant to polishing), yields better quality EBSD patterns (Figure 2b-c, white arrow) and has a sharp and straight interface with the rest of the grain. This very small zone may be a remnant of a larger zone and could correspond to a recrystallized part or primary zoning within the grain. This observation suggests that the grain may have been more extensively broken and abraded than is apparent. The EBSD data obtained from this grain show no evidence of significant systematic deformation (Figure 2c-d).

Six analyses (including one from Nemchin et al., 2008) give a consistent concordia intercept and weighted mean $^{207}Pb/^{206}Pb$ age (Figure 3a). The weighted mean age is 4364 ± 5 Ma (MSWD = 1.10). One analysis (60-4-5, Table 1) is slightly discordant on the concordia diagram, but gives the same $^{207}Pb/^{206}Pb$ age. This may be an artifact as the analysis was made in the centre of the grain following four previous analyses around the margins. The outer analyses could have modified the conductivity in the centre of the grain inducing a change in the extraction of U and Pb and therefore a slight shift of the U-Pb ratio. The U content and the Th/U are consistent throughout the grain, varying between 100 and 128 ppm and 0.58 and 0.62 respectively (Table 1). The consistent age of 4364 ± 5 Ma is interpreted as the age of igneous crystallization of the zircon.

4.2. Zircon 73235,60#5 – 'the cracker'

This rectangular subhedral zircon grain (Figure 4a) is ~120 µm long, and forms part of a small granophyric clast composed of silica and ternary feldspar (Meyer et al., 1996). Grain fractures are filled by feldspar and the zircon has inclusions of feldspar and quartz, suggesting it crystallized at the same time as the granophyre. This is in agreement with Meyer et al. (1996) who interpreted the age of the zircon as a good estimate of the age of the clast given the "close textural relationship between the zircon and the granophyric clast". Variations in polishing relief and EBSD pattern quality identify several irregular domains of low crystallinity (Figure 4b-c). The grain is fragmented by brittle fractures, several of which have measurable offsets. EBSD mapping shows that the fragments of the grain have consistent internal crystallographic orientation, yet are misoriented relative to each other (Figure 4c). Cumulative misorientation across the grain is about 24º (Figure 4c).

Five new U-Pb analyses (including one from a different, smaller grain in the same lithic clast, numbered 60-5-5, Figure 4a) are consistent with data obtained by Nemchin et al. (2008) and Meyer et al. (1996), and show a spread of $^{207}Pb/^{206}Pb$ ages between 4219 ± 5 Ma (spot 60-5-9, Meyer et al., 1996) and 4175 ± 7 Ma (spot 60-5-2) (Figure 3b). Excluding the youngest age, which is obtained in a spot partly overlapping a low crystalline domain and a number of intersecting cracks in the zircon, a mean $^{207}Pb/^{206}Pb$ age is obtained at 4208 ± 8 Ma (MSWD = 2.5). This age is in good agreement with the concordia model age (Ludwig, 1998) at 4207 ± 6 Ma (MSWD = 0.13). The Th/U values vary between 0.29 and 0.43, while U and Th range between 73 and 130 ppm and 21 and 56 ppm, respectively. On the basis of consistency of the ages throughout the grain, we interpret the age of 4208 ± 8 Ma as the age of igneous crystallization of the zircon.

4.3. Zircon 73235,59#3 – 'the tiger'

This zircon grain is one of the largest in the studied grains, measuring about 220 x 180 µm (Figure 5a-b). It is a well rounded, anhedral clast enclosed in the breccia matrix. The centre of the grain is dark in CL and preserves subtle, complex pattern of discontinuous and irregular bands (Figure 5c). Two domains, with sharp

and irregular interfaces with the rest of the grain, occur at its rim: they have high polish relief, stronger EBSD patterns and are bright in CL (Figure 5, white arrows). EBSD reveals that the CL pattern is spatially associated with a progressive crystallographic misorientation across the grain of ~4° across the grain (Figure 5e). This misorientation is gradational and not accommodated by discrete boundaries at the angular and spatial resolution of the data (~0.5°, 1μm). In addition, planar features identified in the optical microscope images are also visible in the EBSD pattern quality image (black arrows, Figure 5d).

Eleven analyses acquired within the main part of the zircon (including two of Nemchin et al. (2008) and two analyses obtained earlier at the ANU; Table 1) spread along the concordia ranging from 4395 ± 11 Ma and 4331 ± 7 Ma (Figure 3c). This variation in the ages does not appear to be correlated with the deformation of the grain or with the CL pattern. The weighted average of 4354 ± 8 Ma (n = 11) has a high MSWD of 4.8, as a result of the spread of individual analyses. The concordia intercept age is 4354 ± 11 Ma (MSWD = 5.2). A single analysis (spot 59-3-7) on the narrow, bright-CL domain at the edge of the zircon yields an age of 4106 ± 18 Ma (95% conf. level), which is ~250 m.y. younger than the main part of the zircon. The inner, dark-CL part of the grain yields U and Th contents of 51-82 ppm and 25-47 ppm, respectively, and Th/U ranging from 0.49 to 0.58. The bright-CL domain on the rim has significantly lower concentrations of U and Th of 19 ppm and 7 ppm, respectively, and Th/U of 0.36. Although it is possible that the main body of the zircon has experienced minor Pb loss, the weighted average age of 4354 ± 8 Ma is interpreted as the best estimate of the age of igneous crystallization. The 4106 ± 18 Ma low U, bright CL patches on the outer margins of the grain either represent areas of complete loss of radiogenic Pb and most U or are from a later overgrowth.

4.4. Grains 73235,60#2 and #3

Zircon grains 73235,60#2 and 73235,60#3 are relatively small, featureless in BSE images and have rounded shapes indicating mechanical and/or thermal abrasion (Figure 6). These grains do not yield strong enough EBSD patterns to index any mineral phases, with the exception of a small domain on 73235,60#3 (Figure 6e-f). General lack of EBSD pattern indicates that the grains have lost their crystallinity probably due to significant radiation damage.

U-Pb data obtained for these grains are given in Table 1 and Figure 3d-e. The three U-Pb analyses on the zircon grain 73235,60#2 (including one data point from Nemchin et al., 2008) yield very consistent ages. The concordia age (Ludwig, 1998) and the weighted average $^{207}Pb/^{206}Pb$ age are similar within errors, the latter yielding an age at 4347 ± 25 Ma (MSWD = 4.1), interpreted as the igneous crystallization age. The U content is between 173 and 190 ppm, Th is between 92 and 98 ppm and the Th/U is 0.51-0.53.

A total of six U-Pb ages were determined on zircon grain 73235,60#3, including two from Nemchin et al. (2008). These ages range between 4409 ± 13 Ma and 4305 ± 5 Ma. If the youngest age, whose slight reverse discordance origin remains unclear (dashed ellipse, Figure 3e) is excluded, the concordia age (Ludwig, 1998) of the grain is estimated as 4360 ± 18 Ma (MSWD = 0.46). Alternatively, two spots showing older ages of 4409 ± 13 Ma (spot 60-3-2) and 4397 ± 21 Ma (spot 60-3-4) are located in the same part of the grain and can represent an older part of this zircon. The average of these two analyses is 4405 ± 22 Ma (MSWD = 0.25), while the younger three analyses determine an average of 4350 ± 10 Ma (MSWD = 0.18). However, establishing the origin of the age differences is difficult as there is little evidence of internal structure in the grain. The U and Th concentrations range between 103-140 and 48-77 respectively, while Th/U varies from 0.46 to 0.55.

4.5. Grain 73235,80#2

Grain 73235,80#2 is a rounded fragment approximately 90 μm across, with no internal structure visible in CL except several random fractures (Figure 7). The textural homogeneity of the grain is reflected in consistency of U-Pb data. Five spots analyzed within this grain at Australian National University and two analyses published by Nemchin et al. (2008) are nearly concordant (Table 1) and show narrow range of $^{207}Pb/^{206}Pb$ ages between 4328 ± 6 Ma and 4342 ± 4 Ma, with both concordia intercept and weighted average $^{207}Pb/^{206}Pb$ ages similar at 4339 ± 6 Ma (MSWD = 1.3; Figure 3f). U and Th concentrations vary from 14 to 120 and 9 to 73 ppm respectively, while Th/U shows narrow range between 0.59 and 0.60. Given the internal textural and chemical homogeneity of this grain, the age of 4339 ± 6 Ma is interpreted as dating igneous crystallization.

4.6. Previously published data

U-Pb data for two zircons from two lithic clasts found in the thin sections 73235,63 and 73235,82 were discussed by Meyer et al. (1996) and Pidgeon et al. (2007), respectively. These results have been presented by Meyer et al. (1996) and Pidgeon et al. (2007) using different initial Pb corrections. These data, recalculated using Stacey and Kramers (1975) common Pb composition, are presented in Table 2, and differ from those presented in the original papers by no more than 2 m.y.

Meyer et al. (1996) described an equant, rounded, ~60 μm zircon inside a granophyric clast found in thin section 73235,63. Three analyses of this zircon give a weighted average $^{207}Pb/^{206}Pb$ age of 4317 ± 21 Ma (MSDW = 2.4) and an upper concordia intercept age of 4314 ± 23 Ma (MSWD = 1.9). The 4317 ± 21 Ma age is interpreted as dating the time of igneous zircon crystallization in the granophyre. The zircon has relatively high U and Th concentrations ranging from 326 to 430 ppm and from 145 to 219 ppm respectively, while Th/U varies between 0.44 and 0.55.

Pidgeon et al. (2007) investigated a complex zircon aggregate (termed the 'pomegranate' zircon) found in an anorthosite clast from the thin section 73235,82. Two distinct textural domains identified within this zircon define two different ages. Twenty four analyses of crystalline fragments determine weighted average $^{207}Pb/^{206}Pb$ age of 4311 ± 11 Ma (MSWD = 8.9), and concordia intercept age of 4316 ± 18 Ma (MSWD = 4.9). Following the original publication (Pidgeon et al., 2007), the concordia intercept is interpreted as the time of igneous crystallization of both zircon and host anorthosite. Twelve analyses of glassy zircon surrounding the fragments give a weighted average $^{207}Pb/^{206}Pb$ age of 4187 ± 7 Ma (MSWD = 4.7), and concordia intercept age of 4188 ± 8 Ma (MSWD = 3.0); the latter is interpreted to represent modification of this zircon during an impact. U and Th concentrations in the zircon fragments vary from 25 to 106 ppm and from 6 to 52 ppm respectively, while the secondary zircon shows overall higher concentrations of U between 86 and 215 ppm and lower concentrations of Th between 15 and 29 ppm. These variations result in a significant difference between Th/U in fragments (0.40-0.70) and in secondary zircon (0.10-0.26).

5. DISCUSSION

5.1. Significance of U-Pb ages

The interpretation of zircon ages in lunar breccias relies on understanding (i) the textural relationships between the zircon and the surrounding clast or matrix material and (ii) the internal structures of zircon grains. On the Moon, zircon growth is only possible from crystallizing igneous melt, as, in the absence of active tectonics, circulation of metamorphic fluids is limited and does not contribute to zircon growth. Evidence of lunar zircon grown from igneous melt is indicated by the presence of zircon grains in a variety of clasts of both mafic and felsic plutonic rocks (Meyer et al., 1996; Pidgeon et al., 2007; Nemchin et al., 2008). The melt can however be produced by either entirely endogenous processes, such as heat production within a KREEP enriched reservoir, resulting from the last stages of the magma ocean crystallization, or as a result of impacts. Studies of terrestrial impacts indicate that some major collisions, such as one at Sudbury have been accompanied by melting of the crust and an uplift of the underlying mantle (e.g., Grieve et al., 1991). Therefore, it is possible that lunar plutonic magmatism is also connected to major impact events. However, this is still to be demonstrated and in the present discussion, we will refer to impact melt zircon only when texture indicates that the zircon crystallized from an impact melt. All other grains are referred to as magmatic in origin.

Although new zircon on the Moon can only grow from melt (formed by either endogenic processes or impacts), solid-state modification accompanied by partial or complete Pb loss and resetting of the U-Pb system is possible under extreme P-T conditions generated by impacts (e.g., Pidgeon et al., 2007, Nemchin et al., 2009). As a result, it is essential to understand the mechanism of zircon formation and identify subsequent modifications to correctly interpret obtained U-Pb ages. In particular, when two (or more) textural domains with different ages are present within a single zircon grain, it is necessary to determine whether the secondary zircon is a solid-state modification of the existing grain or new zircon grown from an impact melt (e.g., the ‘tiger’ grain). It is equally important to establish whether zircon grains that have a homogenous distribution of ages and structural characteristics grew from a melt or were completely reset by an impact event, especially when the zircon is located in the breccia matrix and the link with the original host rock is missing (e.g., the ‘hexagon’ zircon or 73235,80#2). In some cases where this connection is not present and zircon

grains do not show clear age variability with respect to the internal structure, age interpretation can become ambiguous. As the host breccias are most probably formed during the basin-forming events at ~3.9 Ga, there is always a possibility that these events could have partially reset the U-Pb system of the zircons. However, the internal reproducibility of ages in the zircon grains indicates that the ~3.9 Ga event did not affect their U-Pb systems.

Several zircon grains preserve features that can be used to establish a framework for the interpretation of ages of other zircons found in the lunar breccias. One of these grains is the 'pomegranate' zircon described in detail by Pidgeon et al. (2007). Secondary domains in this zircon are very unlikely to be formed from a melt as the grain is locked in an anorthosite clast with no melt visible near the zircon. As a result, this secondary zircon was interpreted to form as a solid-state modification of a pre-existing (~4.3 Ga) zircon under extreme conditions generated by an impact at about ~4.2 Ga (age given by the secondary domains). Another "important" grain was found in the thin section 72215,195 and described by Nemchin et al. (2009). Some zones along the edges of this grain preserve crystal-plastic deformation microstructure identified by EBSD mapping whereas the relatively undeformed central parts preserve significantly older ages. As a consequence, the U-Pb age of the most deformed domains (called secondary zircon) was interpreted to represent complete Pb loss via deformation-enhanced diffusion during an impact event, and therefore date this impact (Nemchin et al, 2009).

The analysis of these two grains suggests that solid-state modification of a lunar zircon as a result of an impact can be recognized as an extreme deformation of the grain, either forming a pattern of intense crystallographic misorientation, resolved via EBSD (such as that found in the grain from the thin section 72215,195) or resulting in complete loss of crystallinity (such as that observed in the 'pomegranate'). On the contrary, zircons (or zircon parts) with little or no deformation are likely to preserve their primary U-Pb system and indicate an igneous crystallization.

Consequently, grains 73235,60#4 ('the hexagon'), the main part of 73235,59#3 ('the tiger', excluding the youngest zone) and 73235,80#2, showing only minor deformation, date crystallization from an igneous melt. Grain 73235,60#5 ('the cracker') shows however a significant rotation of its different fragments, delimited by major brittle fractures which were most likely associated with incorporation of the grain into the host breccia sample. These individual domains are internally

homogenous, i.e., do not show major deformation. Therefore, the age of the 'cracker' grain is interpreted to date the crystallization of the granophyre clast. Similarly, the zircon within a felsic clast found in the thin section 73235,63 and investigated by Meyer et al. (1996) is tentatively interpreted to date the granophyre crystallization, although structural information for this grain is not available. Grains 73235,60#2 and #3 show very poor quality EBSD pattern, indicative of a significant loss of crystallinity of these grains. As a result, their ages are difficult to interpret with a high degree of confidence. They can represent primary magmatic ages with superimposed radiation damage resulting from their relatively high U and Th content or the loss of crystallinity can result from a complete modification of these grains by impacts, similar to that observed in the 'pomegranate'. However, in the absence of strong unambiguous evidence of an impact-related modification, the ages of these grains are interpreted as igneous crystallization ages. Finally, the bright rims, that are visible in the 'tiger' zircon and significantly younger than the main part of the grain, do not appear to be more deformed than the rest of the grain. Consequently, these rims could have grown as a result of interaction of this grain with an impact melt, more than 200 m.y. after its formation. However, close investigation of U and Th concentrations in the two grains with established history (i.e., the 'pomegranate' zircon and zircon from 72215,195; Pidgeon et al., 2007; Nemchin et al., 2009; see above) indicated that the secondary parts of the zircons, interpreted to form by solid-state modification during impact, consistently show lower Th/U values compared to the primary zircon (Figure 8). A similar decrease is observed in the 'tiger' grain, suggesting that the younger rim could also result from a solid-state recrystallization of parts of the grain during an impact at about 4.1 Ga (age of the rim, analysis 59-3-7, Table 1).

5.2. History of the zircon clasts from the South Massif breccias

A summary of zircon U-Pb ages, combining new results and previously published data (Pidgeon et al., 2007; Nemchin et al., 2008; 2009; Grange et al., 2009) obtained on Apollo 17 South Massif samples is shown in Table 3 and Figure 9. The following interpretations of these ages is based on the textural relationships of zircon with other minerals in the breccias as well as on the internal structures of zircon grains often showing complex deformation and recrystallization patterns (see above).

Zircons from sample 73235 suggests that the clast population in this breccia represents at least three separate magmatic events at (1) 4370-4330 Ma, (2) 4320-4310 Ma and (3) ~4200 Ma (Figure 9). The first event is defined by the ages of five out of eight analyzed grains from this sample ('hexagon'; 'tiger'; 73235,60#2; 73235,80#2 and the 3 youngest analyses of 73235,60#3) which show magmatic ages between 4364 and 4339 Ma. The result obtained for grain 73235,60#3 is more difficult to interpret. It is possible that this grain formed at about 4.4 Ga, as shown by the two oldest analyses (Figure 3). Parts of this grain also show ages with an average of 4350 ± 10 Ma; although the interpretation of this age is not obvious due to the relatively small size of the grain and the lack of internal features that can indicate either a magmatic or an impact-related origin. However, in the absence of impact features, we consider this age to be a magmatic age and include it in the oldest magmatic age group. Regardless of the interpretation of this zircon age, there is a clear indication of a magmatic episode between about 4370 and 4330 Ma preserved in the breccia clast population. The composition of the melt which these zircons crystallized from is impossible to establish as the grains are now located in the breccia matrix. However, the size (>100 μm) and euhedral shape of some of these grains are consistent with slow crystallization in plutonic rocks relatively deep in the lunar crust or upper mantle.

This second younger 4320-4310 Ma period of igneous activity is indicated by two other grains (the 'pomegranate', located within an anorthosite clast and the zircon found in a felsic clast in the thin section 73235,63). These grains and their location within lithic clasts indicate plutonic activity that involved both mafic and felsic magmas. Finally, the third magmatic event is defined by the 'cracker' zircon (73235,60#5), enclosed in a quartz-feldspar clast, yielding an age of 4208 ± 8 Ma. In addition to these three magmatic episodes, the zircon population in sample 73235 also records two impact events at 4187 ± 7 Ma (the 'pomegranate' secondary zircon) and probably at 4106 ± 18 Ma (the 'tiger' secondary zircon). Both predate the ~3.9 Ga event that has generated the host breccia sample.

Detailed analysis of 4370-4330 Ma zircon grains indicates that the magmatic history during this period is probably more complex than just a single pulse of activity. While ages of the 'hexagon', the 'tiger' and zircons 73235,60#2 and #3 cannot be separated within the errors (respectively at 4364 ± 5, 4354 ± 8, 4347 ± 25 and 4350 ± 10 Ma), grain 73235,80#2 appears to be younger (at 4339 ± 6 Ma). This

549 difference of about 10 Ma results in a MSWD of 10 for the average age calculated
550 including all five zircon grains falling within 4370 and 4330 Ma interval (4354 ± 15
551 Ma, Figure 9). Therefore, it is likely that this period is characterized by several
552 distinct intrusions of magma. At least two, at about 4360-4350 (defined by the 4
553 oldest zircons) and at 4340 Ma (defined by 73235,80#2) are supported by the
554 currently available data obtained for the sample 73235. This conclusion is also
555 supported by other samples representing material from the South Massif and collected
556 at Stations 2 and 3 of Apollo 17 landing site. Data obtained for zircon grains from the
557 sample 73217 investigated by Compston et al. (1984) and Grange et al. (2009)
558 indicate that a gabbronorite intrusion crystallized at 4332 ± 7 Ma in the area sampled
559 during the breccia formation. In addition, the majority of U-Pb ages obtained on
560 zircon fragments extracted from the saw dust of Station 2 samples 72255 and 72275
561 fall in the range between 4370 and 4330 Ma (Figure 9; Nemchin et al., 2008).
562 However, these two samples show subtle differences in distribution of zircon ages in
563 this time interval (Figure 9). While approximately a third of the fragments from
564 sample 72255 shows ages of about 4350 Ma, a majority of zircon grains from sample
565 72275 have ages of about 4340 Ma. Although zircons separated from the saw dust
566 samples lack textural context, this small difference supports the interpretation of at
567 least two separate magmatic events (i.e., one at 4360-4350 Ma and another at ~4340
568 Ma) suggested by the present investigation of complex zircons from sample 73235.
569 In addition to providing support of a complex magmatic history between 4370
570 and 4330 Ma, zircon fragments from sample 72255 also record events at about 4.2 Ga,
571 consistent with both magmatic (‘cracker’) and impact related (‘pomegranate’) zircons.
572 Evidence of earliest activity (as old as 4.42 Ga) is given by the primary part of a
573 zircon grain from sample 72215,195 (Nemchin et al., 2009) collected at Station 2
574 from the same boulder as samples 72255 and 72275 (Figure 1d). The secondary part
575 of this same zircon from 72215,195 (Nemchin et al., 2009) as well as an acicular
576 zircon grown in a melt from sample 73217 give a strong indication of an early impact
577 at 4335 Ma (Nemchin et al., 2009; Grange et al., 2009).
578 Combining all zircon ages, together with their textural characteristics and
579 interpretation of their internal structures, obtained from the samples collected at
580 Stations 2 and 3 indicate the following history of material incorporated into the South
581 Massif breccias (Table 3):

1 − The earliest activity recorded in the zircon grains is older than 4.40 Ga and most likely represent a magmatic event (primary zircon from 72215,195; Nemchin et al., 2009);

2 − Several plutonic bodies form between 4370 and 4330 Ma and contain rocks varying in composition from norite and anorthosite to felsite and granophyre (‘hexagon’, primary part of ‘tiger’, 73235,60#2, 73235,80#2, 73217,52#2 and youngest ages from 73235,60#3, this study; Grange et al., 2009);

3 − The earliest impact recorded in the zircon grains takes place at 4335 ± 5 Ma (73217,52 acicular zircon #2 and secondary zircon from 72215,195; Grange et al., 2009; Nemchin et al., 2009);

4 − Another period of plutonic activity occurs between 4320 and 4310 Ma (primary zircon of the ‘pomegranate’ grain and zircon from sample 73235,63; Pidgeon et al., 2007; this study);

5 − A felsic melt is generated at 4208 ± 8 Ma (‘craker’ zircon, this study) and a second significant impact occurs at about the same time (4187 ± 7 Ma; secondary zircon of the pomegranate grain, Pidgeon et al., 2007);

6 − Finally, another impact is recorded at 4106 ± 18 Ma (secondary part of the ‘tiger’ grain, this study);

7 – The clasts are incorporated into the host breccia at ~3.9 Ga, although this event is not seen in the zircon record.

5.3. Implications for the provenance of the South Massif breccias

The complexity of zircon ages measured in the aphanitic breccias from the South Massif raises the fundamental issue of how fragments of such a variety of rocks with different ages can be incorporated into the breccia samples deposited in a single relatively small area. Most of this variation is, in fact, visible in the single sample 73235. The variability of ages of magmatic zircons is relatively easy to explain, as a single, even small region on the Moon, could have experienced a complex magmatic history, similar to that commonly observed in the magmatic provinces on the Earth. This evidence of multiple magmatic events was already pointed out by Ryder et al. (1997) who established a lunar crust cross-section at Apollo 17 landing site, prior to the Serenitatis event. They showed that the crust at the Serenitatis impact site is most likely composed of numerous overlapping intrusions. These intrusions are consistent

with Mg-suite composition, i.e., norite and troctolite at shallow level and few KREEP-rich gabbro deeper in the crust (Ryder et al., 1997).

However, explanation of evidence of three impacts prior to the ~3.9 Ga breccia-forming event, recorded by zircon grains in the analyzed samples, is less obvious. This explanation is intimately linked to the question of whether the last 3.9 Ga event that formed the breccia samples could deliver material from different areas, which have experienced impacts at different times prior to this event, to a single location at the South Massif. If such mixing of clastic components of aphanitic breccias is not feasible in the 3.9 Ga impact, two alternative explanations of zircons recording different impacts can be envisaged: (1) there was a single area near the lunar surface that has experienced three consecutive impacts (four, if the 3.9 Ga event is counted) or (2) zircons (and other clasts) reflecting different impacts were accumulated in a single area prior to 3.9 Ga event as a result of mixing ejecta blankets of different age overlapping each other.

Analysis of ballistic paths of material ejected during an impact (e.g., Ryder et al., 1997) indicates that the mixing of excavated rocks is somewhat limited. Therefore, a single location within the resulting impact ejecta sheets will correspond to a specific localized volume in the source region prior to the impact. On the other hand, although it is possible that all investigated zircon grains crystallized at a similar location during successive magmatic pulses, as described above, the suggestion that this location experienced three impact events, affecting the zircon grains successively and differently, prior to the last ~3.9 Ga impact seems rather improbable. There is an indication that at least two groups of zircons showing different magmatic and impact histories are present in the investigated breccia samples. For example, the interpretation of zircon data from sample 73217 (Grange et al., 2009), supports the suggestion of transport of clast material near the surface prior to ~3.9 Ga event. In this sample, the similar ages of needle-like zircon, grown in quenched impact melt, and zircons formed in a norite was interpreted as indicating formation of plutonic rocks immediately followed by an impact at 4335 Ma. It is likely that clasts from other samples from South Massif, which experienced the 4335 Ma impact (such as sample 72215), were also brought to the surface at this time. However, other samples, such as 73235 studied here, contain 4320-4310 Ma zircons that formed in plutonic rocks after the 4335 Ma impact, in addition to the magmatic zircons older than this impact. They do not show clear evidence of 4335 Ma impact event and are likely to be extracted

from depth either at 4.2 Ga impact recorded in the “pomegranate” zircon or during the 4.1 Ga event, visible in the “tiger” grain. The zircon evidence therefore suggests independent histories for a number of zircon grains prior to 3.9 Ga.

A more compatible interpretation of the observed age variations is that the zircon grains have been transported to a similar site in separate ejecta initiated by at least three different impacts. In this case, zircon grains could have crystallized in separate locations, been excavated from their crystallization site during the relevant impact event and brought to the same locality, which by 3.9 Ga would consist of several older ejecta blankets overlaying each other.

The presence of abundant zircon in the breccias samples indicates that the pre-3.9 Ga impacts must have been located within the Procellarum KREEP Terrane. Zircon crystallization from mafic melts requires a significant enrichment in incompatible elements, including Zr. As a result, there is an apparent link between the presence of KREEP component in the lunar magmas and the presence of zircon in the rocks, such that significant proportion of zircon clasts in the aphanitic breccias samples indicates their provenance within KREEP-rich areas on the Moon. This conclusion is supported by the observation that ferroan anorthosite (FAN, main constituent of the lunar crust) clasts are very rare in the South Massif breccias. The presence of zircon in the aphanitic breccias, however, does not indicate a specific site for the 3.9 Ga event itself, as the suggested accumulation of different ejecta blankets could have happened at any location inside or outside the Procellarum KREEP Terrane. Nevertheless, the Serenitatis basin is located on the outer boundary of this terrane, which suggests that the clasts in aphanitic breccias are not derived locally.

Finally, some speculations can be made regarding the size of impacts that can generate the observed modifications of zircon grains, excavate and deliver them to the same location. However, care should be taken in the interpretations as the quantitative data that could provide a link between the modifications occurring in the zircon during an impact and the intensity of this impact are presently absent. Therefore, the observed modifications cannot be used directly to determine the energy released during impacts and consequently constrain the size of either impactor or crater. While general stability of zircon under high P-T conditions indirectly suggests significant energy of these impacts, the degree of modification observed in a zircon grain would also depend on the relative position of this grain within the excavation cavity as the P-T conditions vary significantly across the area of impact and with depth. However, the

plutonic origin of zircon gives an indirect way of determining the size of a cavity that is required to excavate these rocks from the lunar interior and bring them to the surface. Observation of craters existing on the Moon indicates that craters 20-30 km in diameter are 4-7 km deep and are probably capable of delivering plutonic rocks that crystallized slowly with the zircon grains. However, the deepest volumes of these craters would be mostly homogenized into the central melt sheet, whereas more moderately shocked materials would more likely come from shallower depths near the crater rims. In this case the requisite craters might need to be considerably larger than the 20-30 km, although not necessarily basin-scale (i.e., perhaps in the 100 km range).

In addition, survival of analyzed zircon grains as well as complete absence of any modification of zircons during the ~3.9 Ga event, suggests that they have been located in a region that experienced relatively mild change in P-T conditions as a result of this last event and was located at the periphery of the impact site at the time of the ~3.9 Ga impact. Most likely, the material comprising the clasts of investigated breccia samples have been originally located near the surface and close to the rim of the ~3.9 Ga excavation cavity. It has been then caught in the ~3.9 Ga impact ejecta, mixed with the impact melt and transported to the current location at the top of the South Massif. Subsequent sliding of some of these materials along the slopes of the massif made them available for collection during the Apollo 17 mission.

5.4. Temporal coincidence of plutonic magmatism and impacts

The possibility of a link existing between impacts and intrusive magmatism on the Moon was a subject of discussion since the first samples have been collected by the Apollo missions. It has been suggested that post-LMO (standing for Lunar Magma Ocean) differentiation of lunar crust and upper mantle can be due to slow crystallization of impact melts formed by some early 3.9 Ga basin size collisions rather than endogenous lunar magmatism (e.g., Alfvén and Arrhenius, 1976; Wetherill, 1981; Grieve et al., 1991). Debate in the late seventies led to a general consensus that impact melts do not differentiate to a significant degree. This view was supported by the homogeneity of terrestrial impact melts (Phinney and Simonds, 1977) and the suggestion that impact melts, commonly containing a significant proportion of relatively cold clasts, will cool down quickly (Simonds et al., 1976). However, more recently, Warren et al. (1996) revisited the concept of a possible link

718 between large impact and lunar plutonic magmatism, based on their evaluation of new
719 data obtained for the Sudbury intrusion and the Chicxulub impact structure as well as
720 extensive modeling of impact processes (e.g., Melosh, 1989). Warren et al. (1996)
721 suggested that some large pre-3.9 Ga impacts on the Moon could generate sufficient
722 amount of melt dominated by mantle materials, providing that the mantle is still hot
723 after the LMO crystallization. Such melts could crystallize slowly and differentiate
724 forming rocks indistinguishable from those produced as a result of purely endogenous
725 activity. The mechanism proposed by Warren et al. (1996) does not necessarily imply
726 that impacts were the prime reason for mantle melting. Impacts could either introduce
727 additional heat to increase the temperature above the solidus of a hot mantle or simply
728 initiate separation and focus of already existing mantle melts under the target area.
729 Regardless of existing models of lunar plutonic magmatism, the U-Pb ages of
730 large lunar zircons provide the first evidence of contemporaneous magmatic
731 differentiation and impacts during the period between the LMO crystallization and
732 late ~3.9 Ga basing-forming events. The ages of magmatic pulses and impact related
733 modifications visible in zircon grains cannot be linked directly to specific impacts.
734 For example, the oldest recognized impact at 4335 ± 5 Ma is still younger than some
735 magmatic zircon grains from the Apollo 17 aphanitic breccias. However, as
736 mentioned earlier, it is possible that some information about magmatic and impact
737 history of the Moon is not recorded by zircon in general or is not preserved by the
738 currently available set of zircon grains. It is also possible that data obtained for the
739 zircon grains from Apollo 17 landing site represent a very local environment rather
740 than having global implications. This, however, contradicts the observation that the
741 inferred early igneous event consisting of several distinct intrusions of magma dated
742 between 4370 and 4330 Ga, and recorded in the lunar zircon ages, is in agreement
743 with the Sm-Nd model age of the KREEP reservoir differentiation at 4.36 ± 0.06 Ga,
744 proposed by Lugmair and Carlson (1978). It is also consistent with the ^{142}Nd age of
745 4320^{+40}_{-56} Ma obtained from the study of high-Ti, low-Ti and KREEP basalts (Nyquist
746 et al., 1995) and interpreted to reflect the timing of major mantle differentiation on the
747 Moon. Although, interpretation of these Nd data by both Lugmair and Carlson (1978)
748 and Nyquist et al. (1995) as time of formation of KREEP source is not supported by
749 more recent zircon results (e.g., Nemchin et al., 2009), Nd ages are still likely to
750 reflect a period of major differentiation event in the KREEP source. The similarity of

published Nd ages and U-Pb zircon data obtained for the Apollo 17 breccias suggests a major pulse of KREEP-related magmatism between about 4.37 and 4.30 Ga on the Moon. Although the link between magmatic pulses and impact cannot be unambiguously established on the basis of currently available data and the similarity of ages of magmatic and impact events can still be a coincidence, the identification of impact-modified zircons having ages within this 4.37-4.30 Ga interval indicates a possible link between this magmatic pulse and impacts.

6. SUMMARY AND CONCLUSIONS

The detailed study presented here combining the investigation of internal structures and U-Pb chronology of zircons grains found in lunar breccias identifies a variety of magmatic and impact events preserved by the zircon grains even on the scale of a single sample. This complex history is indicative of the provenance of clastic material incorporated in the breccias.

Such history constrained by the study of samples from Apollo 17 Station 2 and 3 suggests complex magmatic activity between 4.37 and 4.31 Ga. Zircons also record several major impact events, which occurred prior to the late heavy bombardment. These impact events were responsible for the delivery of clastic material (including zircon) from different original localities to a single location where this material was eventually incorporated into the ejecta of a 3.9 Ga impact. While our data indicate a Procellarum KREEP Terrane provenance of the clastic material from the breccia samples, they are not able to specify the event responsible for the formation of the breccias. This could be a different impact from the one that deposited them at the top of South Massif near the Apollo 17 landing site.

The U-Pb zircon data also provide first evidence of contemporaneous pulses of magma generation and impact events between about 4.37 and 4.30 Ga.

Acknowledgements

We want to thank the NASA, and especially the crew of Apollo 17 as none of the samples will be available for the study without their hard work. We are also grateful to Marc Norman, Liu Dunyi and Odette James for their constructive comments that

785 helped improve the paper. MG and NT acknowledge funding from a Curtin Internal
786 Research Grant. Rob Hart is thanked for his assistance with scanning electron
787 microscopy. AN research at Münster University is currently supported by DFG.
788
789
790

REFERENCES

Alfvén H. and Arrhenius G. (1976). Evolution of the Solar System. Washington, D.C., NASA, pp 599.

Cayzer N.J., Odake S., Harte B., and Kagi H. (2008). Plastic deformation of lower mantle diamonds by inclusion phase transformations. *European Journal of Mineraogy*. **20**, 333−339.

Compston W., Williams I.S. and Meyer C. (1984). U-Pb geochronology of zircons from Lunar Breccia 73217 using a sensitive high mass-resolution ion microprobe. *Proceedings of the Lunar and Planetary Science Conference* **14th**, *Journal of Geophysical Research* **89**, B525-B534.

Dalrymple G.B. and Ryder G. (1996). Argon-40/argon-39 age spectra of Apollo 17 highlands breccia samples by laser step heating and the age of the Serenitatis basin. *Journal of Geophysical Research* **101**, 26069–26084.

Dence M.R., Grieve R.A.F. and Plant A.G. (1976). Apollo 17 grey breccias and crustal composition in the Serenitatis Basin region. *Proceedings of the Lunar Science Conference* **7th**, 1821−1832.

Grange M.L., Nemchin A.A., Pidgeon R.T., Timms N., Muhling J.R. and Kennedy A.K. (2009). Thermal history recorded by the Apollo 17 impact melt breccia 73217. *Geochimica et Cosmochimica. Acta* **73**, 3093−3107.

Grieve R.A.F., Stöffler D. and Deutsch A. (1991). The Sudbury Structure: Controversial or Misunderstood? *Journal of Geophysical Research* **96**, E5, 22753–22764.

Haskin L.A., Korotev R.L., Rockow K.M. and Jolliff B.L. (1998). The case for an Imbrium origin of the Apollo thorium-rich impact-melt breccias. *Meteoritics and Planetary Science* **33**, 959–975.

Head J.W. (1979). Serenitatis multi-ringed basin: Regional geology and basin ring interpretation. *Moon and the Planets* **21**, 439–462.

Huber H. and Warren P.H. (2008). Enigmatic, largely granitic 73217: A lunar mixed melt-breccia, but is it impact melt? *Lunar and Planetary Science Conference XXXIX*, Houston, USA, #2405(abstract).

Ishii T., McCallum S. and Ghose S. (1983). Petrological and thermal histories of Lunar breccia 73217 as inferred from pyroxene crystallization sequences,

exsolution phenomena, and pyroxene geothermometry. *Proceedings of the Lunar Science Conference* **13th**, A631-A644.

James O.B. and Blanchard D.P. (1976). Consortium studies of light-gray breccia 73215: Introduction, subsample distribution data, and summary of results. *Proceedings of the Lunar Science Conference* **7th,** 2131−143.

James O.B.. Brecher A., Blanchard D.P, Jacobs J.W., Brannon J.C., Korotev R.L., Haskin L.A., Higuchi H., Morgan J.W., Anders E., Silver L.T., Marti K., Braddy D., Hutcheon I.D., Kirsten T., Kerridge J.F., Kaplan I.R., Pillinger C.T. and Gardiner L.R. (1975). Consortium studies of matrix of light gray breccia 73215. *Proceedings of the lunar Science Conference* **6th**, 547−577.

James O. B., Hedenquist J. W., Blanchard D. P., Budahu J. R., and Compston W., (1978) Consortium breccia 73255: Petrology, major- and trace element chemistry and Rb-Sr systematics of aphanitic lithologies. *Proceedings of the Lunar and Planetary Science Conference* **9th**, 789–819.

Jolliff B.L., Rockow K.M., Korotev R.L. and Haskin L.A. (1996). Lithologic distribution and geologic history of the Apollo 17 site: The record in soils and small rock particles from the highland massifs. *Meteoritics & Planetary Science* **31**, 116–145.

Jolliff B.L., Gillis J.J., Haskin L.A., Korotev R.L. and Wieczorek M.A. (2000). Major lunar crustal terranes: Surface expressions and crust-mantle origins. *Journal of Geophysical Research* **105**(E2), 4197–4216.

Korotev R.L. (1994). Compositional variation in Apollo 16 impact melt breccias and inferences for the geology and bombardment history of the Central highlands of the Moon. *Geochimica et Cosmochimica Acta* **58**, 3931−3969.

Lehockey E.M., Lin Y.-P. and Lepik O.E. (2000). Mapping residual plastic strain in materials using electron backscatter diffraction. In *Electron Backscatter Diffraction in Materials Science,* (eds A.J. Schwartz, M. Kumar and B.L. Adams), Kluwer Academic/Plenum, pp. 247−264.

Leich D.A., Kahl S.B., Kirschbaum A.R., Niemeyer S. and Phinney D. (1975). Rare gas constraints on the history of Boulder 1, Station 2, Apollo 17. *The Moon* **14**, 407–444.

Ludwig K.R. (1998). On the treatment of concordant uranium-lead ages. *Geochimica et Cosmochimica. Acta* **62**, 665−676.

857 Ludwig K.R. (2003a). User's manual for Squid 1.02. Berkeley Geochronology
858 Center, Special Publication, 74pp.
859 Ludwig K.R. (2003b). User's manual for Isoplot 3.00. Berkeley Geochronology
860 Center, Special Publication No 4, 71 pp.
861 Lugmair G.W. and Carlson R.W. (1978). The Sm-Nd history of KREEP. *Proceedings*
862 *of the Lunar and Planetary Science Conference* **9th**, 689−704.
863 Marvin U.B. (1975). The boulder. *The Moon* **14**, 315–326.
864 Melosh H.J. (1989). Impact cratering: A geologic process. New York, Oxford
865 University Press, pp 245.
866 Meyer C., Williams I.S. and Compston W. (1996). Uranium-lead ages for lunar
867 zircons: Evidence for a prolonged period of granophyre formation from 4.32 to
868 3.88 Ga. *Meteoritics & Planetary Science* **31**, 370−387.
869 Nemchin A.A., Pidgeon R.T., Whitehouse M.J., Vaughan J.P. and Meyer C. (2008).
870 SIMS U-Pb study of zircon from Apollo 14 and 17 breccias: Implications for
871 the evolution of lunar KREEP. *Geochimica et Cosmochimica. Acta* **72**,
872 668−689.
873 Nemchin A., Timms N., Pidgeon R., Geisler T., Reddy S. and Meyer C. (2009)
874 Timing of crystallisation of the lunar magma ocean constrained by the oldest
875 zircon. *Nature Geoscience* **2**(2), 133−136.
876 Nyquist L.E., Wiesmann H., Bansal B., Shih C.-Y., Keith J.E. and Harper C.L.
877 (1995). ^{146}Sm-^{142}Nd formation interval for the lunar mantle. *Geochimica et*
878 *Cosmochimica Acta* **59**(13), 2817−2837.
879 Pidgeon R.T., Furfaro D., Kennedy A.K., Nemchin A.A. and van Bronswijk W.
880 (1994). Calibration of zircon standards for the Curtin SHRIMP. *8th*
881 *International Conference on Geochronology, Cosmochronology and Isotope*
882 *Geology* Berkeley, US Geol. Surv. Circ. 1101, pp 251.
883 Pidgeon R.T., Nemchin A.A., van Bronswijk W., Geisler T., Meyer C., Compston W.
884 and Williams I.S. (2007). Complex history of a zircon aggregate from lunar
885 breccia 73235. *Geochimica et Cosmochimica Acta* **71**, 1370−1381.
886 Prior D.J., Mariani E. and Wheeler J. (2009). EBSD in the Earth Sciences:
887 applications, common practice and challenges. In *Electron Backscatter*
888 *Diffraction in Materials Science* (eds A.J. Schwartz, M. Kumar, B.L. Adams
889 and D.P. Field) Springer, 2nd edition, pp. 345−360.

890 Phinney W.C. and Simonds C.H. (1977). Dynamical implications of the petrology and
891 distribution of impact melt rocks. In *Impact and explosion cratering* (eds.
892 Roddy D.J., Pepin R O. and Merrill R.B.). New York, Pergamon, 771–790.
893 Reddy S.M., Timms N.E., Pantleon W. and Trimby T. (2007). Quantitative
894 characterization of plastic deformation of zircon and geological implications.
895 *Contributions to Mineralogy and Petrology* **153**, 625−645.
896 Reddy S.M., Timms, N.E. and Eglington, B.M. (2008). Electron backscatter
897 diffraction analysis of zircon: A systematic assessment of match unit
898 characteristics and pattern indexing optimization. *American Mineralogist* **93**,
899 187–197.
900 Ryder G. (1993). Catalog of Apollo 17 rocks, Volume 1 − Stations 2 and 3 (South
901 Massif). Lunar and Planetary Institute Office of Curator #87, JSC#26088, 411
902 pp.
903 Ryder G., Stoeser D.B., Marvin U.B., Bower J.F. and Wood J.A. (1975) Boulder 1,
904 Station 2, Apollo 17: Petrology and petrogenesis. *The Moon* **14**, 327–357.
905 Ryder G., Norman M.D. and Taylor G.J. (1997). The complex stratigraphy of the
906 highland crust in the Serenitatis region of the Moon inferred from mineral
907 fragment chemistry. *Geochimica et Cosmochimica Acta* **61**(5), 1083−1105.
908 Rockow K.M. and Haskin L.A. (1996). Why are Apollo 17 impact-melt breccias
909 assigned a Serenitatis origin: a brief critical review. *Lunar and Planetary*
910 *Science Conference XXVII*, Houston, USA, 1089–1090(abstract).
911 Salpas P.A, Lindstrom M.M. and Taylor L.A. (1988). Highland materials at Apollo
912 17: Contributions from 72275. *Proceedings of the 18th Lunar and Planetary*
913 *Science Conference*, 11–19.
914 Schaeffer O.A., Warasila R. and Labotka T.C. (1982). Ages of Serenitatis breccias.
915 Lunar and Planetary Science Conference **13th**, Houston, USA, 685–686
916 (abstract).
917 Simonds C.H. (1975). Thermal regimes in impact melts and the petrology of the
918 Apollo 17 Station 6 boulder. *Proceedings of the Lunar and Planetary Science*
919 *Conference* **6th**, 641–672.
920 Simonds C.H.,Warner J.L., Phinney W.C. and McGee P.E. (1976). Thermal model for
921 impact breccia lithification: Manicouagan and the Moon. *Proceedings of the*
922 *Lunar and Planetary Science Conference* **7th**, 2509–2528.

923 Spudis P.D. and Ryder G. (1981). Apollo 17 impact melts and their relation to the
924 Serenitatis basin. In: Multi-ring basins: Formation and evolution *Proceedings of*
925 *the Lunar and Planetary Science Conference* **12A**, 133−148.
926 Stacey J.S. and Kramers J.D. (1975). Approximation of terrestrial lead isotope
927 evolution by a two-stage model. *Earth and Planetary Science Letters* **26**, 207–
928 221.
929 Stöffler D., Ryder G., Ivanov B.A., Artemieva N.A., Cintala M.J. and Grieve R.A.F.
930 (2006). Cratering History and Lunar Chronology. In: New Views of the Moon.
931 *Reviews in Mineralogy and Geochemistry,* Mineralogical Society of America
932 **60**, Chapter 5, 519–596.
933
934 Timms N.E., Healy D., Reyes-Montes J.M., Collins D.S., Prior D.J. and Young R.P.
935 (2010). The effects of crystallographic anisotropy on fracture development and
936 acoustic emission in quartz. *Journal of Geophysical Research* **115**, B07202, 19
937 pp.
938 Tucker A.T., Wilkinson A.J., Henderson M.B., Ubhi H.S. and Martin J.W. (2000).
939 Measurement of fatigue crack plastic zones in fine grained materials using
940 electron backscattered diffraction. *Materials Science and Technology* **16**,
941 457−462.
942 Warren P.H. and Wasson J.T. (1979). The compositional-petrographic search for
943 pristine nonmare rocks: Third foray. *Proceedings of the Lunar and Planetary*
944 *Science Conference* **10th**, 583−610.
945 Warren P.H., Taylor G.J., Keil K., Kallemeyn G.W., Rosener P.S. and Wasson J.T.
946 (1983). Sixth foray for pristine nonmare rocks and an assessment of the
947 diversity of lunar anorthosites. Proceedings of the 13th Lunar and Planetary
948 Science Conference Part 2, *Journal of Geophysical Research,* **88**, A615−A630.
949 Warren P.H., Claeys P. and Cedillo-Pardo E. (1996). Mega-impact melt petrology
950 (Chicxulub, Sudbury, and the Moon): Effects of scale and other factors on
951 potential for fractional crystallization and development of cumulates. In *The*
952 *Cretaceous-Tertiary Event and Other Catastrophes in Earth History* (eds.
953 Ryder G., Fastovsky D. and Gartner, S.). Boulder, Colorado, Geological Society
954 of America Special Paper 307.
955 Wetherill G.W. (1981). Nature and origin of basin-forming projectiles. In *Multi-ring*
956 *basins* (eds. Schultz P.H. and Merrill, R.B.). New York, Pergamon, 1–18.

957 Wilkinson A.J. (2000). Measuring strains using electron backscatter diffraction. In
958 *Electron Backscatter Diffraction in Materials Science*, (eds A.J. Schwartz, M.
959 Kumar and B.L. Adams), Kluwer Academic/Plenum, pp. 231−246.
960 Williams I.S. (1998). U-Th-Pb geochronology by ion microprobe. In: McKibben
961 M.A., Shanks W.C., Riley W.I. (Eds), Applications of microanalytical
962 techniques to understanding mineralising processes. *Reviews in Economic*
963 *Geology* **7**, 1−35.
964 Winzer S.R., Nava D.F., Schuhmann P.J., Lum R.K.L., Schuhmann S., Lindstrom
965 M.M., Lindstrom D.J. and Philpotts J.A. (1977). The Apollo 17 "melt sheet":
966 Chemistry age and Rb/Sr systematics. *Earth and Planetary Science Letters* **33**,
967 389–400.
968 Wolfe E.W., Bailey N.G., Lucchitta B.K., Muehlberger W.R., Scott D.H., Sutton R.L.
969 and Wilshire H.G. (1981) The geologic investigation of the Taurus-Littrow
970 Valley: Apollo 17 landing site, U.S. Geol. Survey Prof. Pap. 1080, 280 pp.
971 Wood J.A. (1975). The nature and origin of boulder 1, Station 2, Apollo 17. *The*
972 *Moon* **14**, 505-517.
973

LIST OF TABLES

Table 1 SHRIMP U-Pb data

Table 2 SHRIMP U-Pb data of previously published work and recalculated with Stacey and Kramers (1975) common lead.

Table 3 Summary of zircon ages related to specific event

FIGURE CAPTIONS

Figure 1 (a) Map of the Apollo 17 landing site region and traverse between South and North Massifs done by the astronauts for sampling. The numbers indicate the stations where they stopped. Stations 2 and 3 are highlighted. LM: Lunar Module landing site. **(b)** Panorama of Station 3 (photos number AS17-138-21156 to AS17-138-21168), with locations of samples of interest for this study. Locations of boulders and samples are after Ryder (1993). **(c)** Panorama of Station 2 (photos number AS17-138-21069 to AS17-138-21072). **(d)** Details of boulder 1 of Station 2 with location of samples of interest for this study (photo number AS17-138-21030). Panoramas and photos are available at *http://www.lpi.usra.edu/resources/apollo/catalog/70mm/magazine/?138* and *http://www.lpi.usra.edu/resources/apollopanoramas/*.

Figure 2 Images of zircon grain 73235,60#4 (the hexagon) **(a)** BSE image showing the zircon within the surrounding matrix composed of plagioclase (plg) and clinopyroxene (cpx). The location of the SHRIMP spots are indicated with the number n that correspond to analyses 60-4-n of Table 1. **(b)** SE image of the zircon, the white arrow indicates the zone with a slighty different texture. The deepest pit correspond to the SHRIMP spot #60-4-6, and the other ones remain from a preliminary study by C. Meyer. **(c)** EBSD pattern quality map shown as band contrast from poor (black) to good (white). **(d)** Cumulative misorientation map derived from EBSD pattern shown in degrees from the reference point (red cross) as indicated in the colour scale. Scale bar is 50 μm.

Figure 3 Concordia diagrams of the zircon grains analysed within sample 73235. **(a)** zircon 73235,60#4 'the hexagon'. **(b)** zircon 73235,60#5 'the cracker'. **(c)** zircon 73235,59#3 'the tiger'. **(d)** 73235,60#2. **(e)** 73235,60#3, the white and grey ellipses indicated the two age group identified within the grain. **(f)** 73235,80#2.
The ages reported on the figure are the $^{207}Pb/^{206}Pb$ weighted averages given at the 95% confidence level ('mean age'). Ellipses drawn in dashed lines have been excluded from the calculation of the weighted averages (see text for detail). Error ellipses are shown at the 2σ level.

Figure 4 Images of zircon grain 73235,60#5 (the cracker). **(a)** BSE image showing the 'cracker' and two smaller nearby zircon grains (zrc) and their relationship with the felsic clast and the surrounding matrix. The location of the SHRIMP spots are indicated with the number n that correspond to analyses 60-5-n of Table 1, the spots n=6 and n=7 are after Nemchin et al. (2008). The exact location of the spots from Meyer et al. (1996) is not known (n=8 and n=9). The white rectangle shows the position of Figure 2b-d. **(b)** SE image of the biggest zircon grain. The deepest pits correspond to the SHRIMP spot #60-5-6 and -7 (Nemchin et al., 2008), and the shallower one is one made by Meyer et al. (1996). **(c)** Cumulative misorientation map derived from EBSD pattern shown in degrees from the reference point (red cross) as indicated in the colour scale. Except for (a), scale bar is 50 μm.

Figure 5 Images of zircon grain 73235-59#3 (the tiger). **(a)** BSE image showing the zircon grain within the matrix. The location of the SHRIMP spots are indicated with the number n that correspond to analyses 59-3-n of Table 1, the spots n=9 and n=10 are after Nemchin et al. (2008) but their respective exact position is not known; the two other shallower pits represent also some ion probe analyses made during preliminary work by C. Meyer. The white arrows indicate the textural variation within the grain. **(b)** SE image of the zircon, the arrows indicate the variation in relief of the two parts of the grain. **(c)** CL image of the grain showing the compositional difference between the two parts (the whitish circles are remnants of ion probe pits of preliminary work); the difference in contrast showing irregular bands can be seen at the top of the grain above the right arrow. **(d)** EBSD pattern quality map shown as band contrast from poor (black) to good (white); the white arrows show the higher crystalline quality of the small edges of the grain; the black arrows point to the planar features ("tiger stripes"). **(e)** Cumulative misorientation map derived from EBSD pattern shown in degrees from the reference point (red cross) as indicated in the colour scale. Scale bar is 100 μm.

Figure 6 Images of small zircon grains from sample 73235-60 **(a)** BSE image showing the zircon 73235,60#2 within the matrix and the locations of the SHRIMP spots (Table 1). **(b)** SE image of the zircon 73235,60#2, the small pit is the spot number 60-2-3. Not EBSD data were obtained for this grain. The lighter squares visible on the grain correspond to zones scanned with the SEM to test the quality of

EBSD response. **(c)** BSE image showing the zircon 73235,60#3 within the matrix. The very bright phase is gold remaining in the small cracks after the polishing. **(d)** SE image of the zircon 73235,60#3; the dashed line represent the approximate boundary between the zone of the zircon that shows an EBSD pattern and the zone that cannot be indexed by the EBSD on figures (e) and (f). **(e)** EBSD pattern quality map shown as band contrast from poor (black) to good (white), the white line shows the contour of the zircon grain. **(f)** Cumulative misorientation map derived from EBSD pattern shown in degrees from the reference point (red cross) as indicated in the colour scale. The scale bar is 50 μm.

Figure 7 Images of 73235,80#2. **(a)** CL and **(b)** BSE images of the grain. No EBSD values are available for this grain. The scale bar is 50 μm.

Figure 8 Diagram of Th/U versus the age of some zircon grains showing two parts with different ages, the youngest parts of each grain (square) have lower Th/U than the oldest (circle). White: the 'tiger' grain (73235,59#3); Grey: the oldest lunar zircon (72215,195); Black: the 'pomegranate' grain (73235,82).

Figure 9 U-Pb ages obtained on zircon from the Apollo 17 landing site. Impact and magmatic events are those identified in Table 3. Data are after Meyer et al. (1996), Pidgeon et al. (2007), Nemchin et al. (2008, 2009) and Grange et al. (2009).

Table(s)

Table 1: SHRIMP U-Pb results for zircon of breccia 73235

Samples	U	Th	$^{232}Th/^{238}U$	Th/U	$^{206}Pb/^{204}Pb$	$^{207}Pb/^{206}Pb$	err %	$^{208}Pb/^{206}Pb$	err %	$^{238}U/^{206}Pb$	err %	^{204}Pb corrected (d) $^{207}Pb^*/^{206}Pb^*$	err %	$^{238}U/^{206}Pb^*$	err %	$^{207}Pb^*/^{206}Pb^*$
Zircon-spots	(ppm)	(ppm)				total	1σ	total	1σ	total	1σ		1σ		1σ	(age Ma)
73235,59																
zircon #3 - tiger																
59-3-1	53	27	0.52	0.50	47130	0.5451	0.54	0.129	0.92	1.045	1.72	0.5449	0.55	1.045	1.72	4368 ± 8
59-3-2	51	25	0.51	0.49	11740	0.5557	0.76	0.126	1.06	1.086	1.73	0.5552	0.76	1.088	1.73	4395 ± 11
59-3-3	62	34	0.56	0.55	8390	0.5459	0.30	0.140	0.87	1.064	1.71	0.5452	0.30	1.067	1.71	4368 ± 4
59-3-4	82	47	0.60	0.58	46660	0.5398	0.25	0.148	0.71	1.058	1.69	0.5397	0.25	1.059	1.69	4353 ± 4
59-3-5	71	40	0.59	0.57	50780	0.5404	0.29	0.146	0.83	1.119	1.70	0.5405	0.29	1.119	1.70	4356 ± 4
59-3-6	67	39	0.60	0.58	10590	0.5322	0.50	0.151	0.76	1.069	1.70	0.5316	0.50	1.071	1.70	4331 ± 7
59-3-7*	19	7	0.37	0.36	10620	0.4569	0.61	0.098	1.79	1.176	1.83	0.4562	0.61	1.178	1.84	4106 ± 9
59-3-8	79	46	0.60	0.58	447980	0.5373	0.27	0.148	0.76	1.084	1.69	0.5373	0.27	1.084	1.69	4347 ± 4
59-3-9 (3-1) (a)	63	36	0.58	0.57	19970	0.5365	0.43	0.145	0.74	1.012	1.09	0.5362	0.43	1.013	1.12	4344 ± 6
59-3-10 (3-2) (a)	64	37	0.58	0.58	33760	0.5403	0.33	0.146	0.73	0.999	1.10	0.5402	0.33	1.000	1.11	4355 ± 5
59-3-11 (1.1) (b)	48	24	0.54	0.50	4082	1.0976	0.54			1.098	1.10	0.5394	0.54	1.103	1.10	4353 ± 8
59-3-12 (1.2) (b)	78	48	0.61	0.62	2451	1.0828	0.43			1.083	0.98	0.5353	0.43	1.091	0.98	4341 ± 6
73235,60																
zircon #2																
60-2-1	182	94	0.54	0.52	33170	0.5354	0.32	0.130	0.82	1.013	1.71	0.5352	0.32	1.014	1.71	4341 ± 5
60-2-2	190	98	0.53	0.51	160390	0.5425	0.39	0.132	0.83	1.031	1.71	0.5425	0.39	1.031	1.71	4361 ± 6
60-2-3 (1-1) (a)	173	92	0.52	0.53	207890	0.5357	0.32	0.132	0.62	1.064	1.13	0.5357	0.32	1.064	1.12	4342 ± 5
zircon #3																
60-3-1	103	48	0.48	0.46	28370	0.5405	0.73	0.118	1.03	1.018	1.80	0.5403	0.74	1.019	1.80	4355 ± 11
60-3-2	130	64	0.51	0.49	620930	0.5604	0.91	0.126	0.97	1.043	1.74	0.5604	0.91	1.043	1.75	4409 ± 13
60-3-3	136	67	0.51	0.49	16800	0.5392	0.60	0.122	1.03	1.040	1.97	0.5389	0.60	1.041	1.97	4351 ± 9
60-3-4	113	52	0.48	0.46	22660	0.5556	1.41	0.115	1.13	1.068	2.13	0.5558	1.41	1.067	2.13	4397 ± 21
60-3-5* (2-1) (a)	140	77	0.54	0.55	72660	0.5221	0.33	0.130	0.57	1.003	1.10	0.5220	0.33	1.004	1.08	4305 ± 5
60-3-6 (2-2) (a)	124	65	0.49	0.52	68260	0.5374	0.55	0.120	0.63	1.015	1.08	0.5374	0.55	1.016	1.09	4347 ± 8
zircon #4 - hexagon																
60-4-1	103	58	0.58	0.57	11430	0.5447	0.36	0.141	1.04	1.025	1.78	0.5442	0.36	1.027	1.78	4366 ± 5

Table 1 *continued*

Samples	U	Th	$\frac{^{232}Th}{^{238}U}$	Th/U	$\frac{^{206}Pb}{^{204}Pb}$	$\frac{^{207}Pb}{^{206}Pb}$	err %	$\frac{^{208}Pb}{^{206}Pb}$	err %	$\frac{^{238}U}{^{206}Pb}$	err %	^{204}Pb corrected [d] $\frac{^{207}Pb^*}{^{206}Pb^*}$	err %	$\frac{^{238}U}{^{206}Pb^*}$	err %	$\frac{^{207}Pb^*}{^{206}Pb^*}$
Zircon-spots	(ppm)	(ppm)				total	1σ	total	1σ	total	1σ		1σ		1σ	(age Ma)
60-4-2	101	57	0.58	0.56	39870	0.5448	0.62	0.145	1.08	1.022	1.78	0.5446	0.63	1.023	1.78	4367 ± 9
60-4-3	100	57	0.59	0.57	9410	0.5462	0.38	0.146	1.08	1.036	1.79	0.5455	0.38	1.038	1.79	4369 ± 6
60-4-4	103	59	0.59	0.57	34890	0.5451	0.37	0.145	1.06	1.044	1.78	0.5450	0.37	1.045	1.78	4368 ± 5
60-4-5	128	73	0.59	0.57	7320	0.5436	0.46	0.144	1.33	1.194	1.78	0.5428	0.46	1.197	1.78	4362 ± 7
60-4-6 (4-1) [a]	107	67	0.60	0.62	53510	0.5397	0.37	0.147	0.68	1.014	1.08	0.5396	0.38	1.014	1.08	4353 ± 6
zircon #5 - cracker																
60-5-1	121	48	0.41	0.39	13340	0.4886	0.33	0.101	1.11	1.117	1.75	0.4881	0.39	1.119	1.77	4206 ± 6
60-5-2*	75	26	0.36	0.34	7280	0.4791	0.44	0.093	1.50	1.110	1.78	0.4782	0.44	1.113	1.78	4175 ± 7
60-5-3	76	22	0.30	0.29	27990	0.4824	0.46	0.081	1.67	1.100	1.96	0.4822	0.46	1.101	1.97	4188 ± 7
60-5-4	80	24	0.31	0.30	30370	0.4905	0.43	0.079	1.60	1.085	1.80	0.4908	0.43	1.084	1.80	4214 ± 6
60-5-5	116	41	0.37	0.36	10920	0.4889	0.36	0.092	1.89	1.109	1.77	0.4882	0.37	1.111	1.77	4206 ± 5
60-5-6 (3-1) [a]	85	28	0.32	0.33	25280	0.4869	0.36	0.079	0.96	1.069	1.12	0.4867	0.36	1.070	1.09	4201 ± 5
60-5-7 (3-2) [a]	82	29	0.34	0.36	70940	0.4888	0.42	0.084	0.94	1.065	1.13	0.4887	0.42	1.065	1.12	4207 ± 6
60-5-8 (1.1) [c]	73	21	0.29	0.29	9710	0.4921	0.49			1.073	2.69	0.4915	0.49	1.074	2.70	4216 ± 7
60-5-9 (1.2) [c]	130	56	0.43	0.43	20000	0.4927	0.37			1.127	2.59	0.4924	0.37	1.127	2.60	4219 ± 5
73235,80																
zircon #2																
80-2-1 (c)	109	66	0.60	0.61	6289	0.5360	0.34			1.090	1.09	0.5352	0.34	1.093	1.09	4341 ± 5
80-2-2 (c)	110	67	0.61	0.61	5747	0.5335	0.43			1.075	1.07	0.5325	0.43	1.078	1.08	4334 ± 6
80-2-3 (c)	115	70	0.60	0.61	10000	0.5308	0.40			1.066	1.07	0.5303	0.40	1.068	1.07	4328 ± 6
80-2-4 (c)	120	73	0.61	0.61	14085	0.5371	0.34			1.062	1.06	0.5367	0.34	1.063	1.06	4345 ± 5
80-2-5 (2-1) [a]	98	57	0.59	0.58	37190	0.5342	0.36	0.140	0.71	1.010	1.09	0.5341	0.36	1.010	1.09	4338 ± 5
80-2-6 (2-2) [a]	94	56	0.60	0.60	57498	0.5356	0.28	0.149	0.67	1.016	1.08	0.5355	0.28	1.016	1.08	4342 ± 4

* data not taken into account for mean age calculation as shown in Table 3

[a] data published in Nemchin et al. (2008) as the name shown in bracket, thin section 73235,59 was named 73235,54 in Nemchin et al. (2008)

[b] data obtained at the ANU by C. Meyer

[c] data published in Meyer et al. (1996) as the name shown in bracket

[d] data corrected for the common lead using Stacey-Kramers model (1975)

Ages are given at 1σ

Table(s)

Table 2: Recalculated results for previously published zircon SHRIMP U-Pb data

Samples	U	Th	$^{232}Th/^{238}U$	Th/U	$^{206}Pb/^{204}Pb$	$^{207}Pb/^{206}Pb$	err %	$^{208}Pb/^{206}Pb$	err %	$^{238}U/^{206}Pb$	err %	^{204}Pb corrected [b] $^{207}Pb^*/^{206}Pb^*$	err %	$^{238}U/^{206}Pb^*$	err %	$^{207}Pb^*/^{206}Pb^*$
Zircon-spots	(ppm)	(ppm)				total [a]	1σ	total [a]	1σ	total	1σ		1σ		1σ	(age Ma)
73235,63 - Meyer et al., 1996																
1.1	472	250	0.51	0.53	8696	0.5217	0.54			1.029	1.85	0.5210	0.54	1.031	1.86	4302 ± 8
1.2	325	149	0.44	0.46	12987	0.5293	0.40			1.032	1.34	0.5289	0.40	1.034	1.34	4324 ± 6
1.3	324	183	0.55	0.56	13514	0.5270	0.25			0.995	1.29	0.5266	0.25	0.997	1.30	4317 ± 4
73235,82 - pomegranate - Pidgeon et al., 2007																
82-p1 (m)	86	23	0.27	0.26	12439	0.4843	0.4	0.065	1.62	1.038	2.77	0.4838	0.39	1.040	2.60	4193 ± 6
82-p2	106	52	0.51	0.49	12052	0.5382	0.349	0.130	0.74	0.991	2.71	0.5377	0.39	0.993	2.48	4348 ± 5
82-p3 (m)	124	27	0.22	0.22	28296	0.4862	0.355	0.059	1.83	1.080	2.69	0.4860	0.39	1.080	2.48	4199 ± 5
82-p4 (m)	94	18	0.19	0.19	24384	0.4783	0.464	0.051	1.65	1.204	2.70	0.4780	0.50	1.205	2.53	4175 ± 7
82-p5	52	27	0.53	0.52	97269	0.5233	0.561	0.135	1.09	1.027	2.85	0.5232	0.59	1.027	2.47	4308 ± 8
82-p6	65	29	0.45	0.44	35768	0.5224	0.574	0.118	1.02	0.999	2.80	0.5222	0.59	1.000	2.60	4305 ± 8
82-p7	62	32	0.52	0.51	19385	0.5247	0.479	0.133	1.00	1.036	2.81	0.5244	0.50	1.037	2.70	4311 ± 7
82-p8 (m)	113	29	0.27	0.26	23702	0.4876	0.39	0.073	1.94	1.078	2.71	0.4873	0.39	1.079	2.48	4203 ± 6
82-p9 (m)	113	18	0.17	0.16	18766	0.4837	0.37	0.040	2.50	1.048	2.71	0.4834	0.39	1.049	2.41	4191 ± 5
82-p10 (m)	147	24	0.17	0.16	26376	0.4814	0.318	0.044	1.96	1.046	2.68	0.4811	0.29	1.047	2.51	4184 ± 5
82-p11 (m)	131	21	0.17	0.16	87669	0.4776	0.336	0.043	1.16	1.065	2.69	0.4775	0.29	1.065	2.45	4173 ± 5
1	25	14		0.56	674	0.5366	0.95			1.098	2.42	0.5280	0.95	1.130	2.49	4321 ± 14
2	61	35		0.57	1439	0.5172	0.58			1.037	2.07	0.5130	0.58	1.051	2.10	4279 ± 9
4	54	31		0.57	1534	0.5291	0.63			1.056	2.11	0.5253	0.63	1.069	2.14	4314 ± 9
5	24	12		0.50	765	0.5216	0.97			1.061	2.44	0.5137	0.97	1.088	2.50	4281 ± 14
6	77	32		0.42	2227	0.5070	0.50			1.091	1.96	0.5042	0.50	1.100	1.98	4254 ± 7
7	18	8		0.44	821	0.5251	1.10			1.110	2.66	0.5178	1.10	1.135	2.73	4293 ± 16
8 (m)	171	27		0.16	4926	0.4772	0.38			1.163	1.74	0.4758	0.38	1.168	1.75	4168 ± 6
9	27	15		0.56	800	0.5345	0.76			1.136	2.04	0.5273	0.76	1.163	2.094	4319 ± 11
10	30	21		0.70	1855	0.5288	0.67			1.010	1.92	0.5257	0.67	1.020	1.94	4315 ± 10
11	36	25		0.69	1536	0.5201	0.72			1.183	2.01	0.5162	0.72	1.198	2.04	4288 ± 11
13	57	32		0.56	1420	0.5280	0.84			0.993	2.28	0.5239	0.84	1.007	2.32	4310 ± 12
14	47	21		0.45	1605	0.5074	1.13			1.064	2.45	0.5035	1.13	1.077	2.48	4252 ± 17
15	62	36		0.58	1139	0.5384	0.86			1.021	2.35	0.5334	0.86	1.039	2.389	4336 ± 13
20 (m)	166	29		0.17	2088	0.4889	0.35			1.231	1.72	0.4857	0.35	1.242	1.74	4198 ± 5

Table 2 *continued*

Samples	U	Th	$^{232}Th/^{238}U$	Th/U	$^{206}Pb/^{204}Pb$	$^{207}Pb/^{206}Pb$	err %	$^{208}Pb/^{206}Pb$	err %	$^{238}U/^{206}Pb$	err %	^{204}Pb corrected (b)				
												$^{207}Pb^*/^{206}Pb^*$	err %	$^{238}U/^{206}Pb^*$	err %	$^{207}Pb^*/^{206}Pb^*$
Zircon-spots	(ppm)	(ppm)				total (a)	1σ	total (a)	1σ	total	1σ		1σ		1σ	(age Ma)
21 (m)	178	28		0.16	4444	0.4798	0.38			1.235	1.73	0.4783	0.38	1.240	1.74	4176 ± 6
22	56	31		0.55	1050	0.5326	0.57			1.152	1.84	0.5271	0.57	1.173	1.88	4319 ± 8
23 (m)	215	22		0.10	4049	0.4815	0.27			1.241	1.74	0.4799	0.27	1.247	1.745	4181 ± 4
24 (m)	92	15		0.16	1812	0.4899	0.41			1.216	1.82	0.4863	0.41	1.229	1.84	4200 ± 6
25	23	12		0.52	429	0.5352	0.90			1.140	2.17	0.5215	0.90	1.192	2.27	4303 ± 13
26	25	14		0.56	1046	0.5267	0.63			1.022	2.45	0.5211	0.63	1.040	2.50	4302 ± 9
27	15	6		0.40	792	0.5329	0.78			1.041	2.60	0.5256	0.78	1.067	2.67	4315 ± 11
28	24	13		0.54	1486	0.5163	0.64			1.019	2.45	0.5122	0.64	1.032	2.48	4277 ± 9
29	61	33		0.54	4525	0.5361	0.39			1.058	2.22	0.5348	0.39	1.063	2.23	4340 ± 6
30	354	24		0.07	3155	0.5321	0.55			1.002	2.30	0.5303	0.55	1.008	2.32	4328 ± 8
31	14	6		0.43	564	0.5327	0.82			1.040	2.70	0.5223	0.82	1.075	2.80	4305 ± 12

(m) indicates analyses obtained on matrix (see text for details)

[a] recalculated from Pidgeon et al. (2007) ANU data

[b] data corrected for the common lead using modern Stacey-Kramers Pb composition (1975)

Ages are given at 1σ

Table(s)

Table 3 : Summary of zircon U-Pb ages obtained for Apollo 17 Stations 2 and 3 breccias

Sample		Thin section	Zircon	Analyses	Reference[a]	Ages (Ma)[b]	error	MSWD	History (see part 5.2.)
Station 3	73235	,59	#3 - tiger	oldest (n=11)	this study	4354	8	4.8	Plutonic bodies 4370-4330 Ma
			#3 - tiger	youngest (n=1)	this study	4106	18	-	Impact
		,60	#2	all (n=3)	this study	4347	25	4.1	Plutonic bodies 4370-4330 Ma
			#3	2 out of 6	this study	4405	22	0.25	-
			#3	3 out of 6	this study	4350	10	0.18	Plutonic bodies 4370-4330 Ma
			#4 - hexagon	all (n=6)	this study	4364	5	1.1	Plutonic bodies 4370-4330 Ma
			#5 - cracker	8 out of 9	this study	4208	8	2.5	Felsic episode
		,80	#2	all (n=6)	this study	4339	6	1.3	Plutonic bodies 4370-4330 Ma
		,82	pomegranate	on fragments n=24	[1]	4316	18	4.9	Plutonic bodies 4320-4310 Ma
			pomegranate	on matrix n=12	[1]	4188	8	3.0	Impact
		,63		all (n=3)	[2]	4317	21	2.4	Plutonic bodies 4320-4310 Ma
	73217	,52	#1	all (n=2)	[3]	4332	7	0.72	Plutonic bodies 4370-4330 Ma
			#2 - needle	all (n=7)	[3]	4335	5	2.5	Impact
Sation 2	72215	,195		oldest (n=4)	[4]	4417	6	0.09	Oldest magmatic activity
				youngest (n=5)	[4]	4333	7	0.04	Impact
	72255	saw cut			[2]				-
	72275	saw cut			[2]				-

[a] mean ages obtained during this study include ages obtained during previous studies (see Tables 1 and 2)

[b] weighted mean $^{207}Pb/^{206}Pb$ age; except for the pomegranate, concordia intercept

[1] recalculated after Pidgeon et al. (2007); [2] Nemchin et al. (2008); [3] Grange et al. (2009); [4] Nemchin et al. (2009)

Errors on ages are given at the 95% conf. level.

Figure(s)

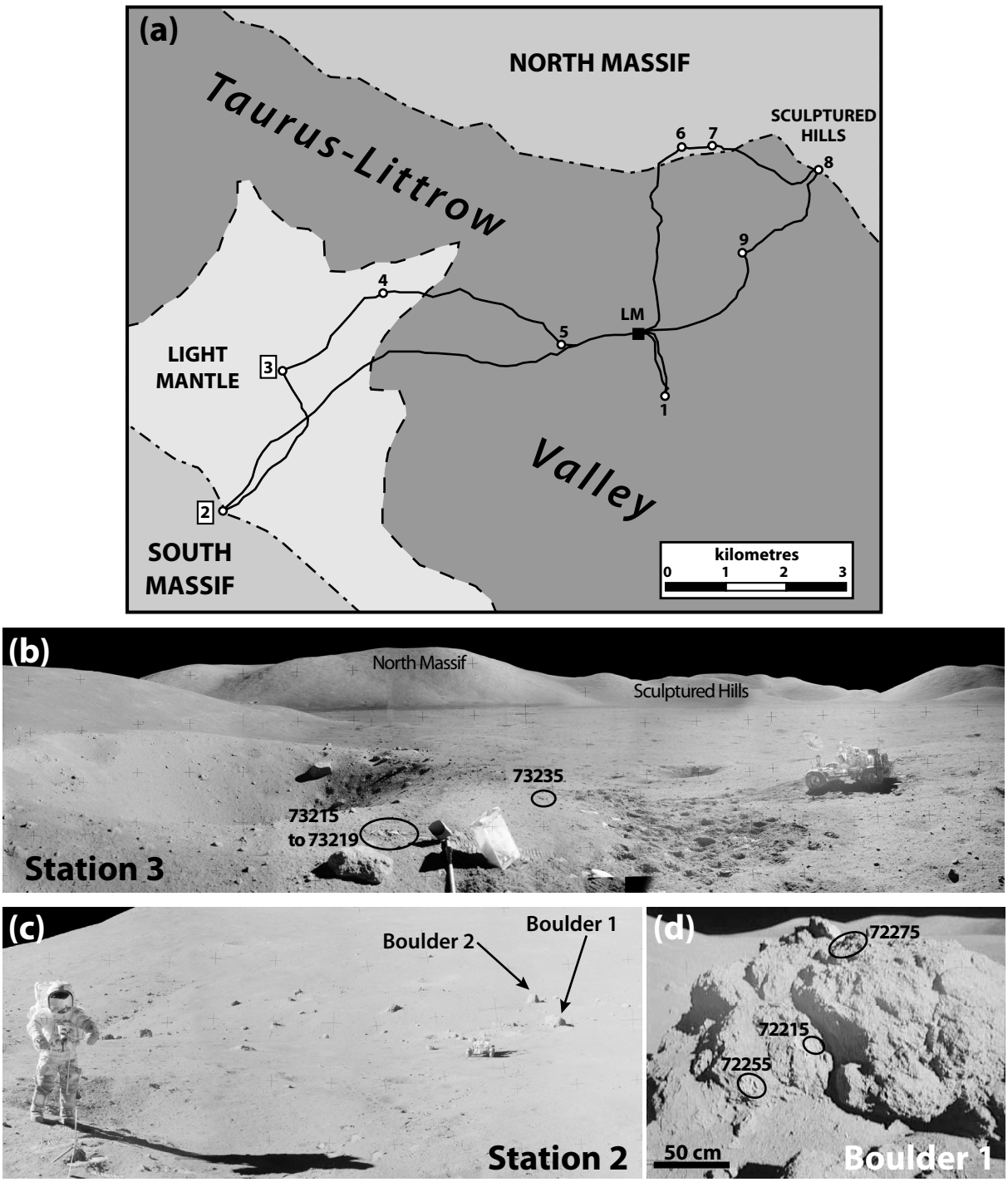
(a)
NORTH MASSIF
Taurus-Littrow
SCULPTURED HILLS
6
7
8
9
4
LM
5
LIGHT MANTLE
3
1
Valley
2
SOUTH MASSIF
kilometres
0 1 2 3
(b)
North Massif
Sculptured Hills
73235
73215 to 73219
Station 3
(c)
Boulder 2
Boulder 1
Station 2
(d)
72275
72215
72255
50 cm
Boulder 1

Figure(s)

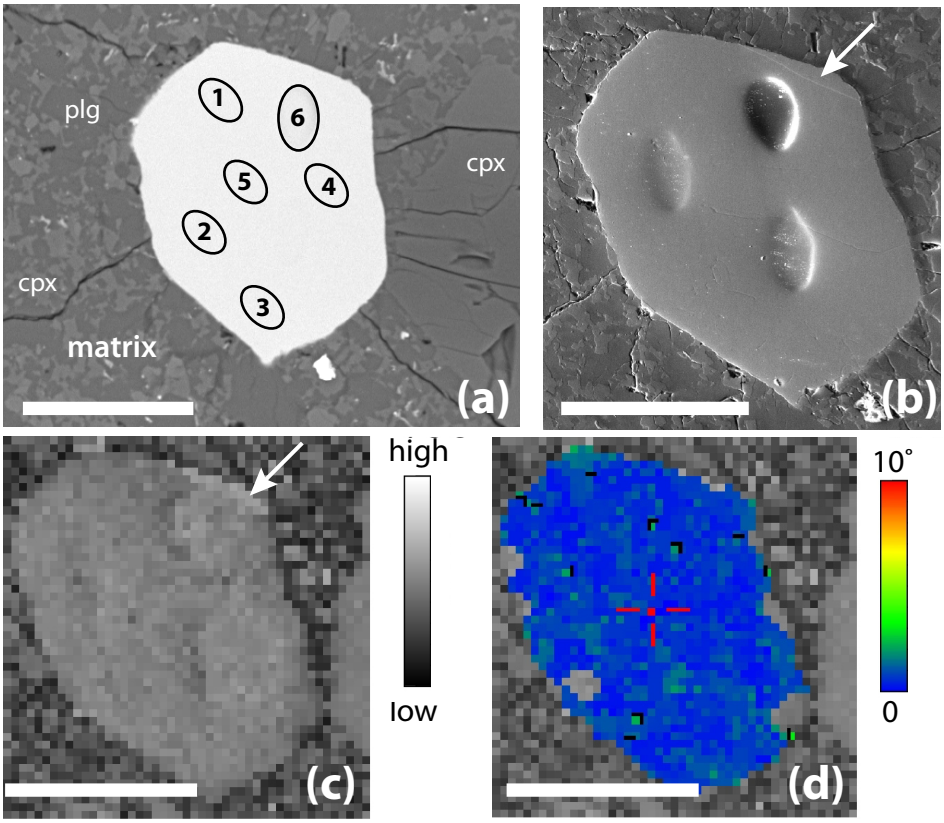

Figure(s)

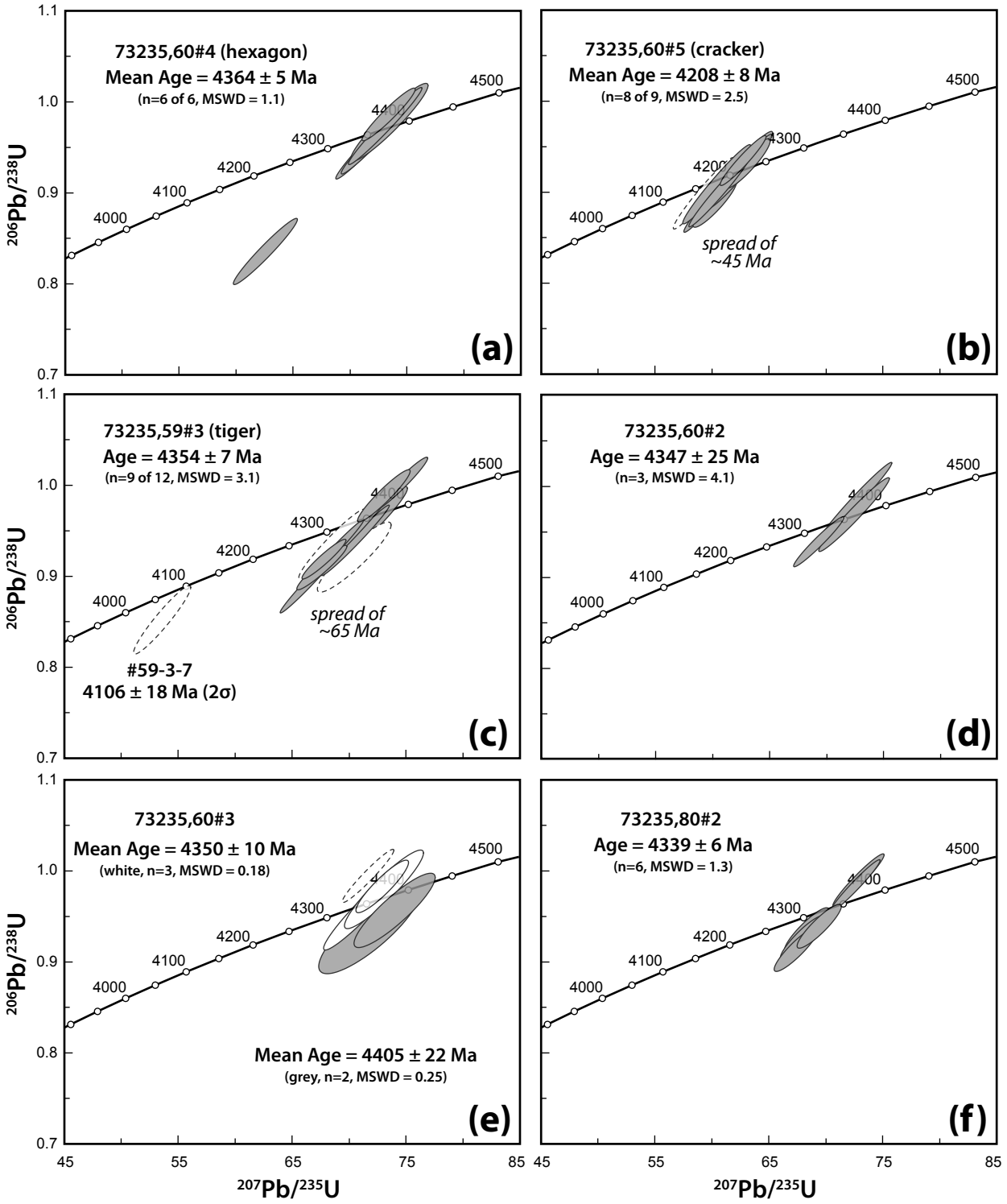
73235,60#4 (hexagon)
Mean Age = 4364 ± 5 Ma
(n=6 of 6, MSWD = 1.1)
(a)
73235,60#5 (cracker)
Mean Age = 4208 ± 8 Ma
(n=8 of 9, MSWD = 2.5)
spread of ~45 Ma
(b)
73235,59#3 (tiger)
Age = 4354 ± 7 Ma
(n=9 of 12, MSWD = 3.1)
spread of ~65 Ma
#59-3-7
4106 ± 18 Ma (2σ)
(c)
73235,60#2
Age = 4347 ± 25 Ma
(n=3, MSWD = 4.1)
(d)
73235,60#3
Mean Age = 4350 ± 10 Ma
(white, n=3, MSWD = 0.18)
Mean Age = 4405 ± 22 Ma
(grey, n=2, MSWD = 0.25)
(e)
73235,80#2
Age = 4339 ± 6 Ma
(n=6, MSWD = 1.3)
(f)
206Pb/238U
207Pb/235U

Figure(s)

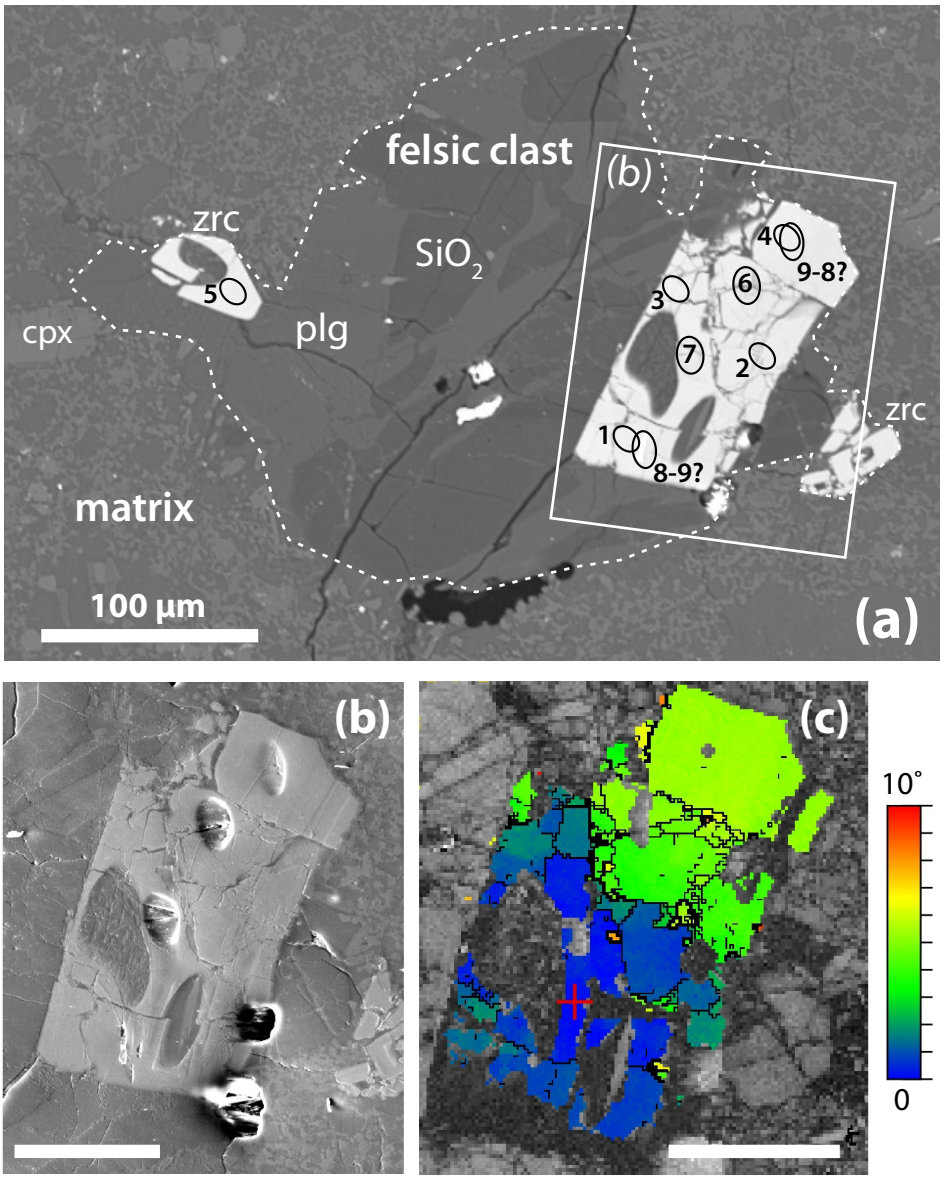
felsic clast
(b)
zrc
SiO2
cpx
plg
matrix
100 µm
(a)
4
9-8?
3
6
7
2
zrc
1
8-9?
5
(b)
(c)
10°
0

Figure(s)

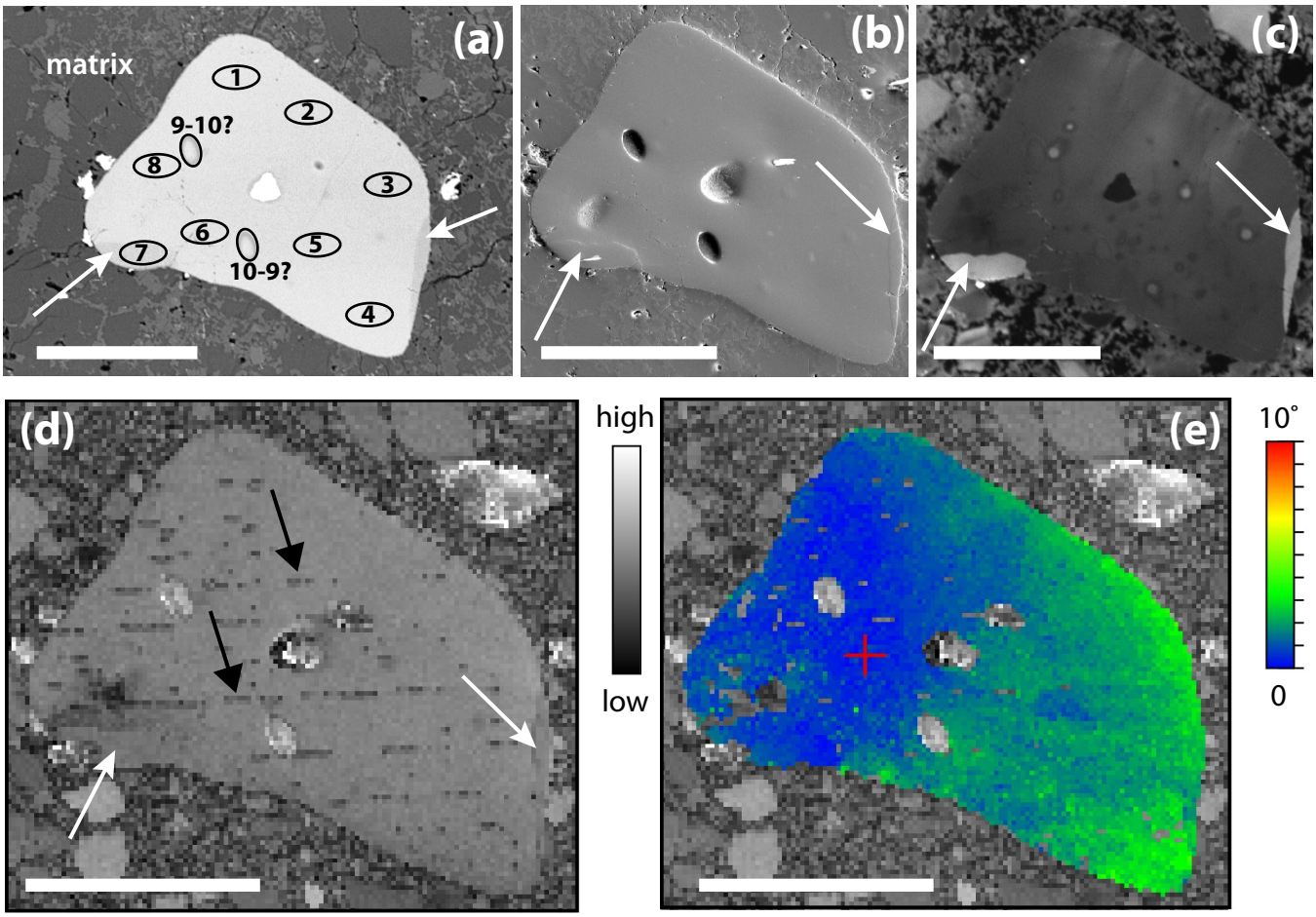

Figure(s)

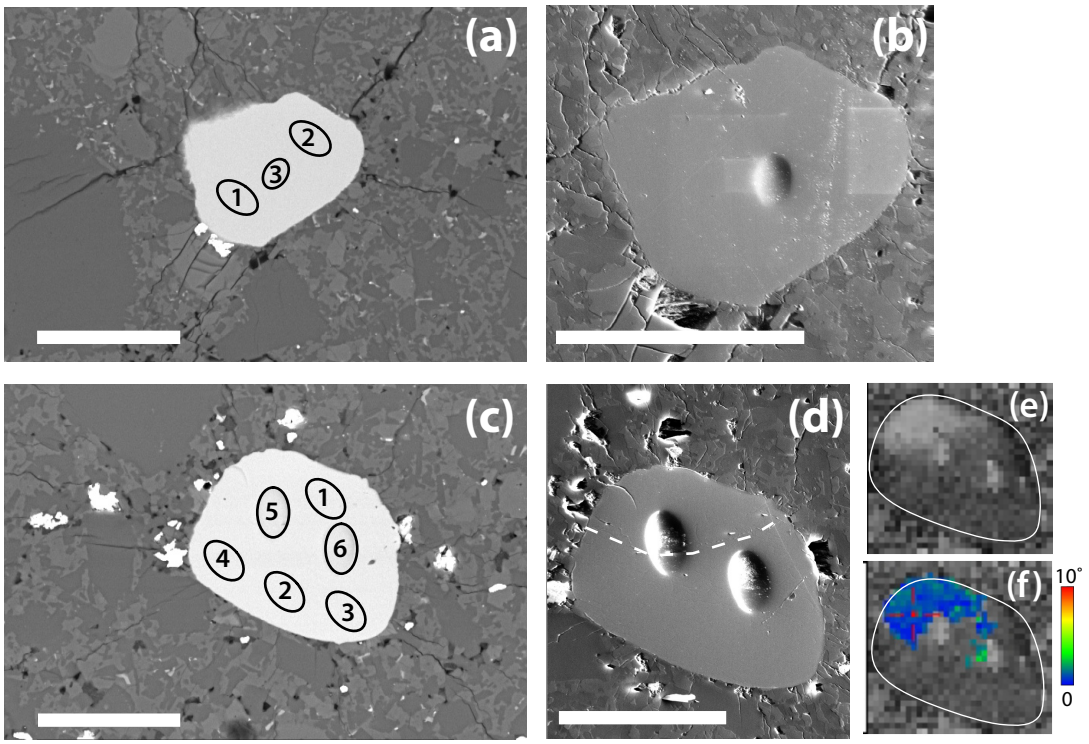

Figure(s)

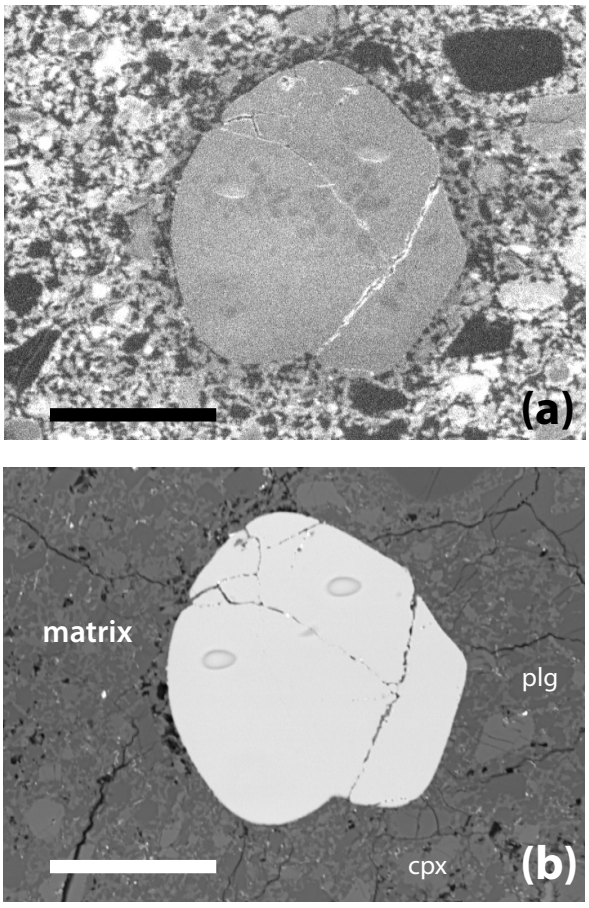

Figure(s)

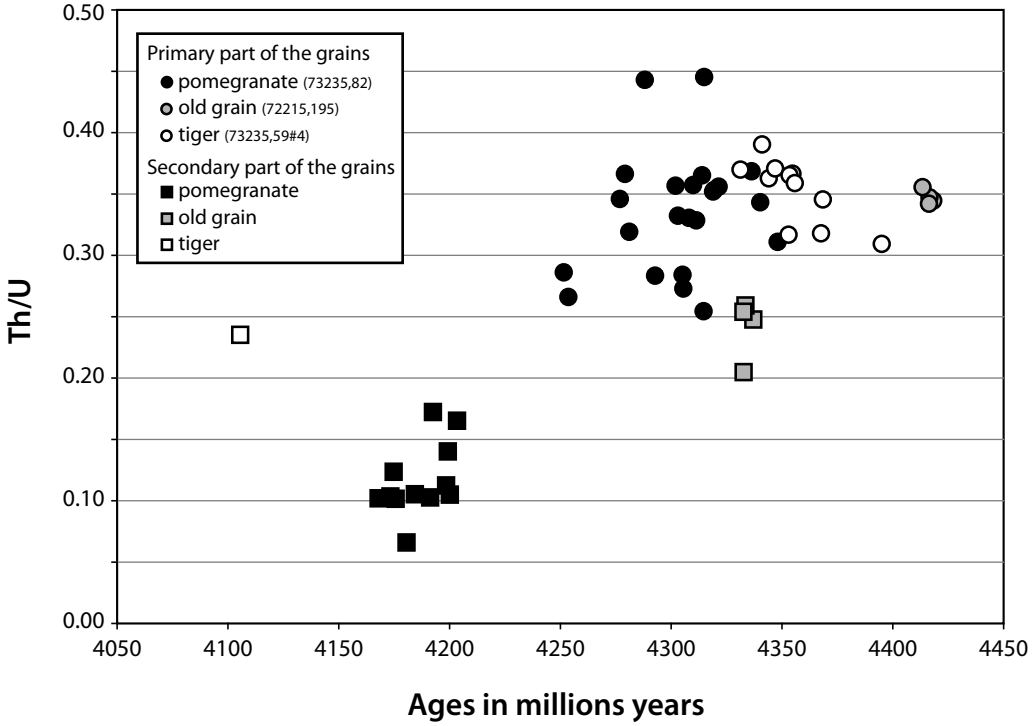
Primary part of the grains
pomegranate (73235,82)
old grain (72215,195)
tiger (73235,59#4)
Secondary part of the grains
pomegranate
old grain
tiger
Th/U
0.50
0.40
0.30
0.20
0.10
0.00
4050
4100
4150
4200
4250
4300
4350
4400
4450
Ages in millions years

Figure(s)

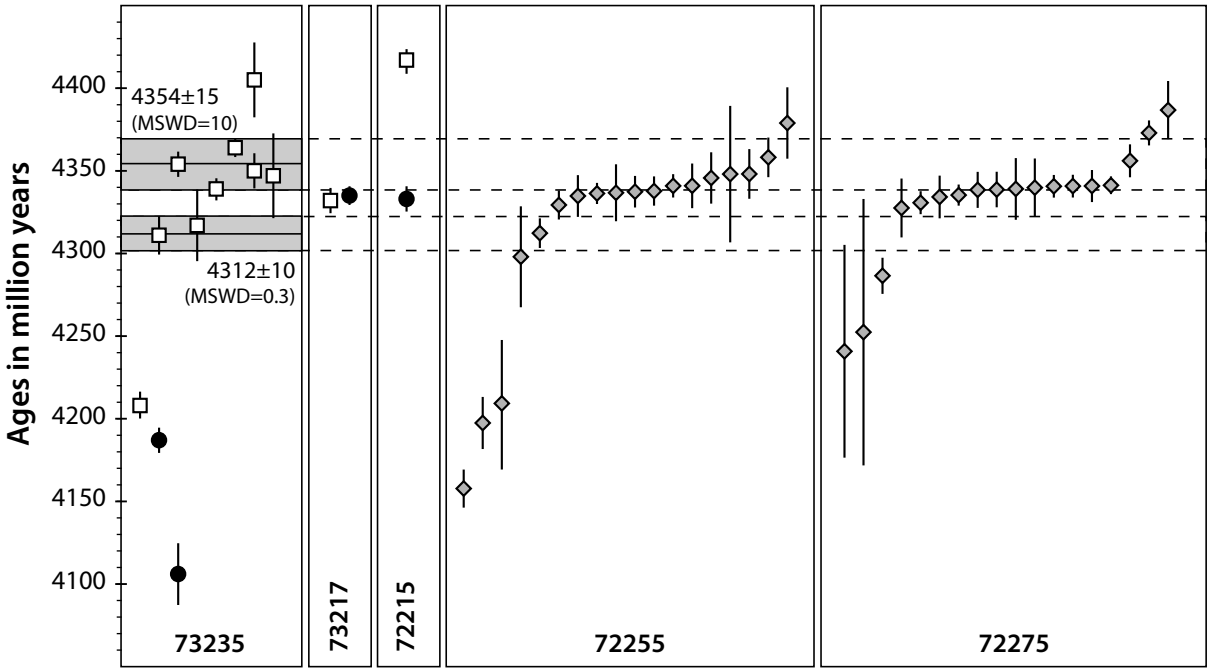
Ages in million years
4400
4350
4300
4250
4200
4150
4100
4354±15
(MSWD=10)
4312±10
(MSWD=0.3)
73235
73217
72215
72255
72275